INVESTIGATION OF TAKE-UP STRUCTURE DESIGN UNDER STEADY AND NON-STEADY CONDITIONS

Greg Wheatley [1]
Rong Situ [2]
Darrin Gangemi [3]
Soheil Keipour [4]

ABSTRACT: This paper is intended for use as a progress report of a potential design for a gravity take-up skid frame. As a result, a new gravity take-up skid frame is required. To obtain the best possible design for the take-up structure, it was separated into four phases. Phase one included concept development of the design. It was found that the motor must be able to handle 132.3 kW of power when the belt is fully flooded. Phase two, the material was selected for the construction. Phase three was the performance analysis of the design. In this stage, calculations justifying design decisions including the conveyor capacity at normal and maximum conditions as well as start-up and shutdown conditions and an analysis of the belt tensile forces at steady and non-steady conditions. The drive system was also analyzed to determine the resistive forces and subsequent power needed to operate the system. Furthermore, the design analysis of the drive, pulleys, idlers and bearings was conducted. Phase four was the FE analysis of the system. This included static analysis on the structure including both the skid frame and take-up weight structure and a fatigue analysis on the pulleys. From this it was determined that the design will operate with the required strength and serviceability as outlined in AS 4100 and AS 3990 for the agreed upon system lifetime. Furthermore, it was determined that the system will operate as required for all agreed upon conditions, that is normal, maximum, start-up and shutdown operating conditions.

KEYWORDS: Skid Frame, Conveyor, Mine Site

[1] Senior lecturer, College of Science & Engineering, James Cook University, Townsville, Australia - greg.wheatley@jcu.edu.au

[2] Senior lecturer, College of Science & Engineering, James Cook University, Townsville, Australia, rong - situ@jcu.edu.au

[3] MSc. Student, College of Science & Engineering, James Cook University, Townsville, Australia - darrin.gangemi@my.jcu.edu.au

[4] Postgraduate, Faculty of Mechanical and Mechatronics Engineering, Shahrood University of Technology, Shahrood, Iran - soheil.keipour@gmail.com

1 INTRODUCTION

In an automation demands efficiency, and conveyors are one technology to enhance the productivity of processing lines. Automation is now a prime driver behind the way products are produced. Many applications include both manual processes and robotic interaction (KHAN et al., 2017, and PATIL et al., 2015, and BARITKAL et al., 2015). Collaboration doesn't necessarily result in custom conveyor designs because after all, standards offerings are less costly than custom. But good supplier recommendations are typically based on using standard products as much as possible while integrating custom designs where needed to ensure reliability and flexibility. That's why a one-size-fits-all conveyor isn't always the best choice.

The goal of a well-designed conveyor system is to serve the process and not to fit the process to the conveyor (DAKHOLE et al., 2012, and SIVAKIMAR et al., 2013). Conveyor equipment selection is a complex, and sometimes, tedious task since there are literally hundreds of equipment types and manufacturers to choose from. The expert system approach to conveyor selection provides advantages of unbiased decision making, greater availability, faster response, and reduced cost as compared to human experts. Conveyor types are selected on the basis of a suitability score, which is a measure of the fulfillment of the material handling requirements by the characteristics of the conveyor. The computation of the score is performed through the Weighted Evaluation Method, and the Expected Value Criterion for decision making under risk. The prototype system was successfully validated through two industrial case studies (FONSECA et al., 2004). A simplified approach to modeling the rolling contact phenomena that occur at the surface of a wheel driven rubber belt (NUTTALL et al., 2006).

The main aim of this approach is to determine the rolling friction due to hysteresis and the relationship between traction and slip in wheel driven belt conveyors. The resulting model is an expansion of an existing linear viscoelastic model consisting of a three parameter Maxwell model combined with a Winkler foundation that is used to determine the rolling friction due to hysteresis in a conventional conveyor with a flat belt. The design of a multi-conveyor system in supporting machine loading and unloading has become crucial to management (LAN et al., 2003).

This study not only mediates the concept of balancing the number of parallel machines, the conveyor speed for adjacent pallets, the overall relevant costs and the determination of the number of conveyors into the objective, but also develops a two-staged method to optimize the combined problem to reach a maximum profit. This paper contributes an applicable scheme for production design in manufacturing, and provides a valuable tool to conclusively obtain the optimal profit of a given production quantity for operations research engineers in today's manufacturing with profound insight.

Over the years a lot of work has done and is still continuing with great effort to save weight and cost of applications. The current trend is to provide weight/cost effective products which meet the stringent requirements (SHINDE et al., 2012). The aim of this paper is to study existing conveyor system and optimize the critical parts like roller, shafts, C-channels for chassis and support, to minimize the overall weight of assembly and material saving. A study of new design of rollers focused on the measurement of static and dynamic resistance of rotating rollers and the impact of new construction on the power consumption of the belt conveyor (OPASIAK et al., 2014). Measurements of static and dynamic resistance of rotating rollers were made on a universal rollers stand.

2   CONCEPT DEVELOPMENT

In order to obtain the best possible design for the take-up structure, a concept development process was undertaken. In this process, the following components were considered. The motor, gearbox and clutch which was sized according to the proceeding power equations. The tensioning method and configuration was then developed. Influence on the designs were taken from Australian Standards and research on the matter.

The final design incorporated as many positive aspects that a reasonably possible when maintainability, constructability, practicality and safety are taken into account. Further justification of the designs is achieved through power calculations where possible. The following sections detail the concept development including power calculations used to justify drive motor selection, development of the design and decision-making process in obtaining the final design as well as specification of idlers.

Next, the pulleys and take-up method were specified. This was achieved through calculations as referenced from (STANDARD DIN 22101, 2011-12). Idlers were then specified using the Lorbrand idler catalogue. The following is the subsequent processes used.

2.1   POWER CALCULATIONS

The following calculations were as per (ME4521: Bulk Materials Handling, 2019). The required power should be large enough to overcome frictional effects and the increasing potential energy of the material. The overall resistance to motion of the belt is separated into various components of resistance. These are as follows: Main Resistances, Secondary Resistances, Special Main resistances, Special secondary Resistances, Slope Resistances.

Effective tension is the sum of the individual components:

$$F_e = F_H + F_N + F_{S1} + F_{S2} + F_{St} \quad (1)$$

Motor power is given by:

$$P_m = \frac{F_e v}{\eta} \quad (2)$$

Where η is motor efficiency and v is belt velocity. Tensile forces in an operating conveyor belt vary with the length of the belt and will change when the belt is stopped, started or during change in product feed rate. To determine suitable belt and counterweight the maximum tension and minimum tension are required. Key belt forces loading the driver are as follows:

$$Maximum\ Tension: F_{max} = F_1 = \zeta F_e \left(\frac{1}{e^{\mu\varnothing} - 1} + 1 \right) \quad (3)$$

$$Minimum\ Tension: F_2 = F_1 - F_e \quad (4)$$

Where F_1 is Carrier side tension, F_2 denotes Return side tension, F_e is effective tension, Ç denotes the dynamic loading factor (1.3 < Ç < 2), ø is Pulley wrap angle and µ is coefficient of friction belt and drive motor. For a belt with a rubber cover layer of rubber lagging it is recommended that (0.4 < µ < 0.45) under dry operating conditions (STANDARD DIN 22101, 2011-12).

The minimum tension is an important factor in relation to conveyor system design. The minimum tension must be large enough to prevent slippage on the drive pulley, and to prevent excess sagging between idler pulleys. Carrier side and return side sage tension are given by:

$$Carrier\ Side: T_{sag} = k_s L_{IC}(m_b + m_s)g \quad (5)$$

$$Return\ Side: T_{sag} = k_s L_{IR} m_b g \quad (6)$$

Where L_{IC} denotes idler spacing on carrier side, L_{IR} is idler spacing on the return side, m_b is belt mas per unit length, m_s denotes bulk mass per unit length and k_s is sag factor. Here it is assumed sag to be within 3%, therefor $k_s = 4.2$.

2.2 DRIVE MOTOR SELECTION

2.2.1 MOTOR

The motor is expected to be able to power the conveyor under normal operating conditions as well as adverse conditions. A motor efficiency of 85% was chosen as motors typically reach peak efficiency within this range as well as it maximizes the motor's life. As recommended in (GOLKA et al., 2007), an allowance of 10% is added to the required power. Therefore, the DRN315L4 AC Motor 400V, 60Hz, 4-pole from SEW-EURODRIVE meets the power requirements of the conveyor, with a rated power of 160 kW.

2.2.2 GEARBOX

The Gearbox power tables from (GEAR SELECTION, 2019) are used to determine the gearbox size. The power and torque needed for the driven machine should be less than the nominal power and torque the gearbox can transmit to allow the gearbox to operate safely. Therefore, the gearbox selected is the DGL2-450 from Dissan.

2.2.3 CLUTCH

A backstop is necessary in the drive system to prevent the reversal on the incline conveyor section. AC motors from SEW-EURODRIVE can have a back stop integrated into the design upon request.

2.3 TENSIONER CONCEPT DEVELOPMENT

2.3.1 DESIGN 1

The initial design (Figure 1) was based on the design put forward in AS4024.3611 for a general gravity take-up system. The design consists of a head pulley positioned at the end of the conveyor, three bend pulleys, a drive pulley and the take-up pulley. From the power calculations observed in Section 2.1, it can be seen that the power necessary in the drive pulley is independent of the pulley positioning and hence is not a significant factor in the design development. What

is important however is the wrap angle of the belt on the drive pulley. An increased wrap angle increases the frictional forces on the belt and hence decreases the amount of weight needed to tension the belt. With this roller arrangement, bend pulleys can be easily positioned to maximize the wrap angle and hence minimize the tensioning forces necessary. However, this arrangement requires extra pulleys compared to other designs which is a disadvantage from a maintenance and construction point of view.
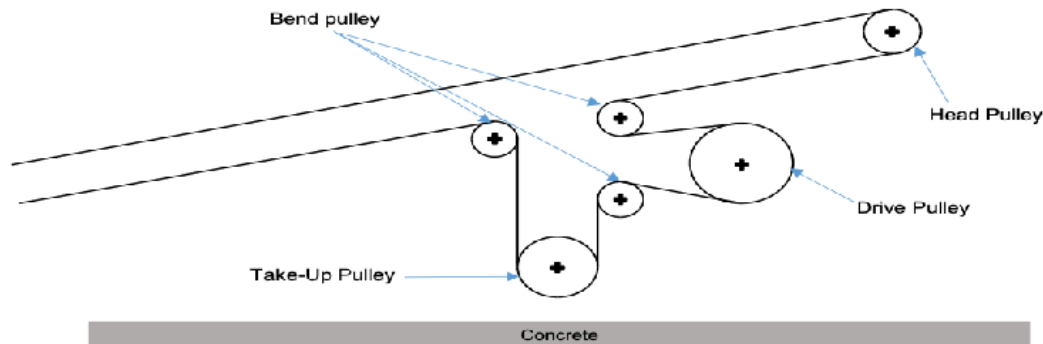

Figure 1 - Concept Design 1

When analyzing this design from a construction, operation and maintenance point of view further advantages and disadvantages are identified. A large advantage of this design is that the drive pulley is on the clean side of the belt. This will allow optimal operation of the conveyor system with no interference that would be generated from a dirty belt. This, however, is largely the only advantage of this system, which is more likely suitable to conveyors of larger dimensions than what this project is constrained to. Disadvantages of this system are largely seen from a construction and maintenance perspective.

Firstly, as this system requires a number of rollers to operate, more supporting structure is necessary in this design. This translates to higher capital costs as well as higher replacement costs because more structure is needed hence more structure is prone to failure. Furthermore, with this roller configuration, the drive motor will need to be mounted high above the ground. This will once again result in more support structure as the motor will induce live loads into the structure which will in turn generate large forces and hence stresses.

Further to this point, by mounting the drive motor in this position, maintenance becomes difficult. Although remote lubrication can be implemented, AS4024.3610 states that visual inspection is also a requirement. This will result in the necessity for platforms and stairways or ladders to enable the operator to get into a position that allows visual inspection. This in turn poses further safety risks to the design.

Finally, the vertical alignment of the tensioner pulley also poses issues. Because of the limited space under the conveyor, it may be that with significant use of the belt that the clearances will eventually not be sufficient. If this is the case, costs will be incurred in belt replacement which may be expensive when compared to other design options.

2.3.2 DESIGN 2

Design 2 (Figure 2) was influenced from research on different designs for a gravity take-up system. This design consists of a drive pulley as the head pulley with a snub pulley to increase the wrap angle. Furthermore, bend pulleys are positioned as to allow a take-up pulley to be vertically positioned. As power is independent of roller positioning, once again the design will be

evaluated on its construction, operation and maintenance merits. However, the positioning of the snub pulley allows for a larger wrap angle around the drive pulley which in turn increase frictional forces and hence decreases the take-up weight necessary to tension the belt. Furthermore, this is accomplished with less pulleys than what is necessary in Design 1, hence lessening the structural componentry of the design.
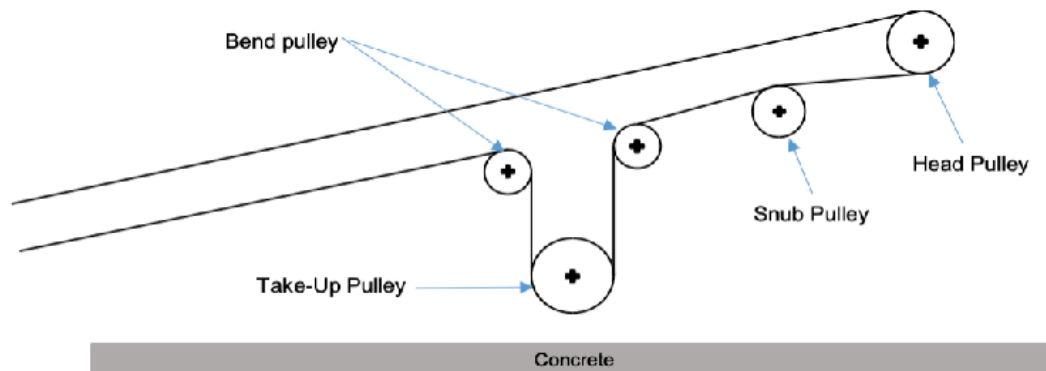

Figure 2 - Concept Design 2

When analyzing the design from a construction, operation and maintenance perspective, further advantages and disadvantages are identified. Firstly, similar to Design 1, the drive pulley is on the clean side of the belt minimizing the need for a scraper. Furthermore, as the drive pulley is also used as the head pulley, the design is subsequently simplified.

However, this characteristic is also indicative of a major design floor of this system, in that the drive motor has to be mounted at the head of the take-up system. This will generate a large torque arm on the system that will require plenty of structural reinforcement to support it. Furthermore, mounting of the drive motor in such a position introduces safety risks into the design. Large exclusion zones will have to be included in the design to prevent personnel from walking under and around the motor. Furthermore, platforms and stairway or ladder systems will also have to be included tom meet the requirements from AS4024.3610 and AS1657.

Also, as the positioning of all pulleys are fairly spread, separate platforms will have to be designed to be able to reach, inspect and maintain all the rollers. Similar to Design 1, the vertical alignment of the take-up pulley may also cause problems in the operation of the system. Once again, as the belt ages it will stretch and hence need more travel distance in the take-up pulley to sufficiently tension it. The limited spacing under the conveyor as a result of the design constraints may limit this.

2.3.3 DESIGN 3

Design 3 (Figure 3) was influenced by research on take-up designs as well as the recommendations of AS4024.3611. It is similar to Design 1 with the rollers reconfigured in such a way that the drive pulley is positioned such that the drive motor can be mounted on the ground. This eliminates the safety issues that were present in the previous two designs. Furthermore, this feature will simplify the design and hence construction of the supporting structures. Furthermore, the pulley positioning is such that the bend pulleys can be positioned to maximize wrap angle on the drive pulley hence decreasing the weight needed to tension the belt. However, contrary to Design 2, more pulleys are required to implement this design which will increase the amount of supports necessary.
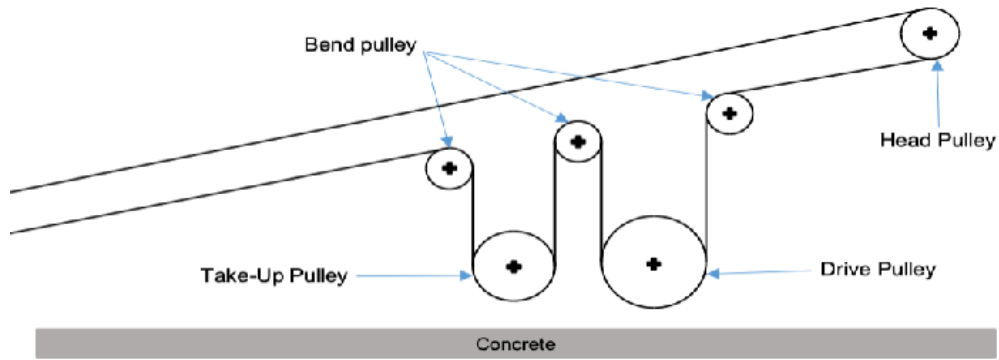
Figure 3 - Concept Design 3

When analyzing the design from a construction, operation and maintenance perspective, similar advantages and disadvantages as identified in the previous two designs are identified. However, there is a clear-cut advantage to the positioning of the drive pulley to the previous designs. Because of its height, the pulley and hence drive motor can be safely and easily operated, maintained and inspected from the ground without the need for elevated platforms and the accompanying stairways or ladders associated with it. This simplifies the design as well as safely implementing the clauses set forth by AS4024.3610.

However, a raised platform will be necessary to be able to safely inspect the bend and head pulleys. Similar to the previous designs, the vertical direction of the take-up pulley may cause issues when the conveyor belt ages and naturally stretches. Because of the constraints on the design, especially the tolerances under the conveyor, eventually, there may not be enough clearance to properly tension the belt.

2.3.4 DESIGN 4

The final take-up design (Figure 4) is based off the design supplied by the clients with some modifications taking the advantages from the previous design as well as fixing the identified disadvantages. This design consists of a head pulley, a drive pulley, two bend pulleys and a horizontally aligned take-up pulley. Like all previous designs, the bend pulleys are positioned as to maximize wrap angle around the drive pulley to maximize the force the drive motor is able to input into the conveyor system as well as minimizing the weight needed in the take-up to tension the belt. Furthermore, the position of the drive pulley is such that the drive motor can be mounted close to the ground minimizing the supporting structure necessary. In addition, this eliminates the safety issues that would arise from mounting the drive motor high above the ground. Another advantage of this configuration when compared to that of the design.
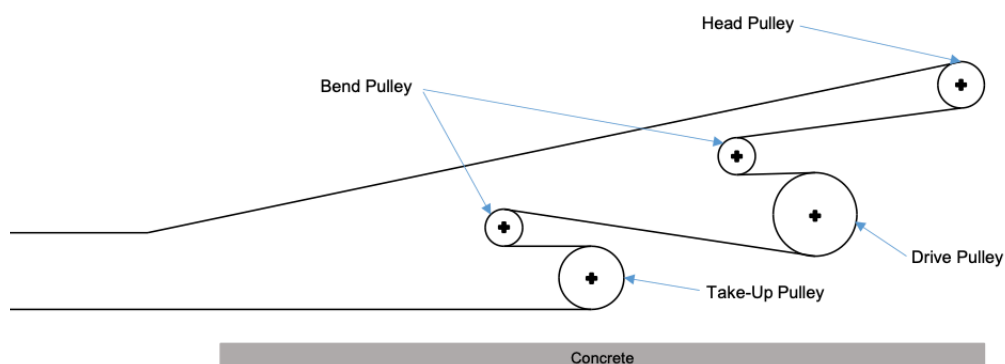

Figure 4 - Concept Design 4

When analyzing the design from a construction, operation and maintenance perspective, the following advantages and disadvantages can be observed. Firstly, construction of the system is simplified as all the rollers are mounted close to the ground. This means that shorter beam lengths can be used which will result in smaller torque arms generated as a result of the forces generated by the rollers on the structural beams. Furthermore, operation and maintenance is simplified as all rollers can be accessed to inspect, lubricate and maintain safely from the ground without the need for raised platforms, meeting AS4024.3610 standards. Furthermore, the alignment of the take-up pulley is superior to that of the previous designs. The horizontal alignment of the pulley means that the space constraint imposed by the conveyor is avoided. Furthermore, as it is a horizontally aligned pulley, safety issues as a result of components under gravitational forces is avoided. Horizontal rails will instead be used to guide the pulley along to tension the belt. Although this will require the use of extra roller bearings, the horizontal alignment is such that it can still be safely inspected and maintained from ground level. This solves the issue previously identified in the preceding designs.

2.3.5 DECISION MATRIX

In order to choose a final design a decision matrix (Table 1) was constructed to aid the decision-making process. Four criteria were selected based on what the client valued most, these being maintainability, constructability, operation and safety. These criteria were weighted so that maintainability was given the highest level of importance, followed by safety and constructability and lastly, operation in the form of the tensioner arrangement. Once again, these weightings were based on client input.

Table 1 - Decision Matrix for Take-Up Arrangement

	Maintainability	Constructability	Tensioner Arrangement (Operation)	Safety	Weighted Total
Weight	9	8	7	8	32
Design 1	6	5	7	6	191
Design 2	6	7	8	5	206
Design 3	7	6	8	6	215
Design 4	8	8	9	7	255

The analyses presented in Sections 2.3.1 to 2.3.4 were done on the basis of the decision matrix criteria which led to Design 4 being selected as the optimal design. Design 4 scored a total of 255 points and was superior to the other designs in all criteria. Design 4 is an adjustment on the design provided by the clients which provides further justification for the design.

With the selection of the design complete, the next stage is to specify materials that will be suitable for such an application as well as further refining the concept through 3D modelling and finite element analysis. Furthermore, the selection of componentry can continue with the specification of idlers, rollers, take-up system and bearings to be used in the design.

2.4 PULLEY SPECIFICATIONS

The following calculations are as per (GOLKA et al., 2007). Refer to Figure 5 for dimension variable definitions.
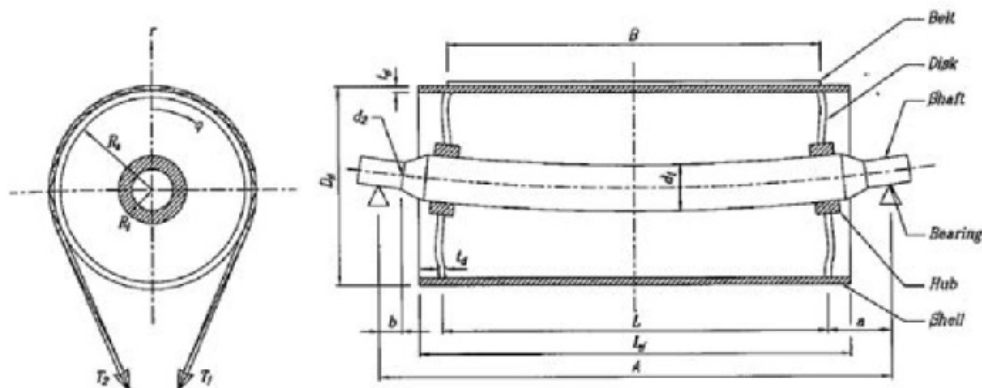

Figure 5 - Pulley Dimensions (GOLKA et al., 2007)

2.4.1 PULLEY SIZING

In order to determine the minimum diameter (D_s) for a pulley the following equations is used:

$$D_s = t_{cs}C_{cs} \quad (7)$$

Where t_{cs} is the belt carcass thickness in mm which for the given belt is 4.6 mm (DUNLOP, 2009) and C_{cs} is a factor dependent on the carcass material which for the given belt is 108. According to the Table 10.3 of (GOLKA et al., 2007), snub pulley diameter can be find.

The minimum pulley face width is dependent on the belt width. To determine the shell thickness two checks must first be made. The first is a stress check which is done using the following equation:

$$t_{s1} = \sqrt{\frac{0.127 k_s p_1 D_s}{F_r}} \quad (8)$$

Where k_s is a safety coefficient which is assumed to be 1.2, p_1 is equal to T_{max}/B, D_S is the pulley diameter and F_r is endurance limit of the shell material. The second check is a buckling check. This is given by:

$$t_{s2} = \sqrt[3]{\frac{(1 - \nu^2)p_2 D_s^3}{2E}} \quad (9)$$

Where ν is Poisson's ratio, E is Young's modulus and p_2 is equal to $2*T_{max}/D_s B$. The greater of these two thicknesses is to be selected. To determine the shaft diameter, torque and bending moment need to be first calculated. Torque is calculated using:

$$T_q = T_e \frac{D_s}{2} 10^{-3} \quad (10)$$

Where T_e is the effective tension. Bending moment is calculated by:

$$M_b = \left(\frac{T_{max}}{2} \right) \frac{(A - l)}{2} \quad (11)$$

Where T_{max} is the pulley total load, A is the distance between bearing centers and l is the distance between disc plates. To then determine the diameter the following equation is used:

$$d_s = \left[\frac{10^4 K_s K}{F_r} \sqrt{M_b^2 + 0.75 T_q^2} \right] \quad (12)$$

Where K is a stress rising factor, F_r is the endurance limit of the shaft material and K_s is a size factor. For simplicity, this same shaft diameter will be used for the snub and take-up pulleys as well.

A safety check-up calculation for the selected locking device, the RINGFEDER Locking Assemblies RfN 7012 is as follows. Equivalent transmissible torque in Nm can be calculated as:

$$T_r = \sqrt{T_q^2 + \left(\frac{\sum F_x D_i}{2} \right)^2} \quad (13)$$

Where T_q is the applied torque, F_x is the sum of axial forces which in this case is zero, therefore, D_i which is the shaft diameter at the locking assembly is irrelevant.

2.4.2 TAKE-UP SPECIFICATIONS

The take-up device of design is a horizontal gravity take-up tensioning method. For the horizontal gravity take-up, the take-up pulley is typically mounted on a trolley and through a series of sheaves is connected to the weight by a steel rope. A schematic of the horizontal take-up tensioning method is showing in Figure 6.
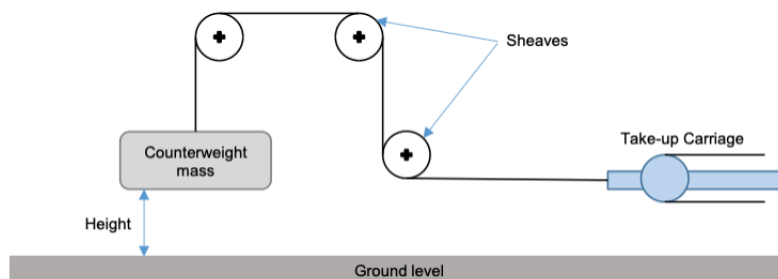
Figure 6 - Horizontal Take-Up Tensioning Schematic

To determine the take-up travel distance the following equation can be used:

$$L_{tu} = L\left(\kappa_{tur} + \kappa_{tus} + \kappa_{tut} + \kappa_{tup} + \kappa_{tuo}\right) + L_{spl} \quad (14)$$

Where L is the conveyor length (800 m), L_{spl} conveyor splicing length (1.5 m) and the k variables are allowances for belt stretch. For a fabric belt, these variables are as follows: k_{tur} Running conditions = 0.016, k_{tus} Starting conditions = 0.002, k_{tut} Thermal length change = 0.005, k_{tup} Permanent stretch = 0.004, k_{tuo} Loose belt allowance = 0.001.

2.5 IDLER SPECIFICATIONS

Selection of carrier idlers was achieved via use of calculations obtained by the Lorbrand Idler Catalogue (www.lorbrand.com). Firstly, the load per station was to be calculated the following was used:

$$Load\ per\ station\ (kg) = S\left(W_b + \frac{Q}{3.6V}\right) \quad (15)$$

Where S is spacing between idler stations, W_b is weight of belt per running metre, Q denotes capacity and V is belt speed.

The next step was to multiply by a participation factor, p. The participation factor is defined as the fraction of the load taken by the roller which experiences the greatest load vs the total station. Figure 7 provides a table of the necessary participation factors.

Station Type	Participation Factor (p)		
	0.42		
	20° 0.65	35° 0.68	45° 0.72
	0.6		
	1		

Figure 7 - Participation Factor Table (www.lorbrand.com)

Selection of return idlers was also achieved using Lorbrand specifications. To determine the load on the return idlers the following was used:

$$F_{return} = 10pS \quad (16)$$

2.6 BEARING

Self-aligning ball bearings were selected as they are commonly used in conveyor systems and because of their superiority over other bearing types. The selected bearings are able to withstand 2.5° of misalignment without affecting bearing performance.

2.7 MATERIAL SELECTION

It is important that the steel selected be of good machinability, weldability and workability. Manufacturability in the form of member section is also an important consideration. Low carbon or mild steel is the selection for the material to be used.

2.8 3D SOLID MODEL

With the concept development complete, a 3D solid model could be designed. The 3D model of the proposed design can be seen in Figure 8. It must be noted, that although not represented in the figures, 40 mm square, 3 mm gauge wire mesh encapsulates the structure. With this in mind, the rest of the design can be justified.
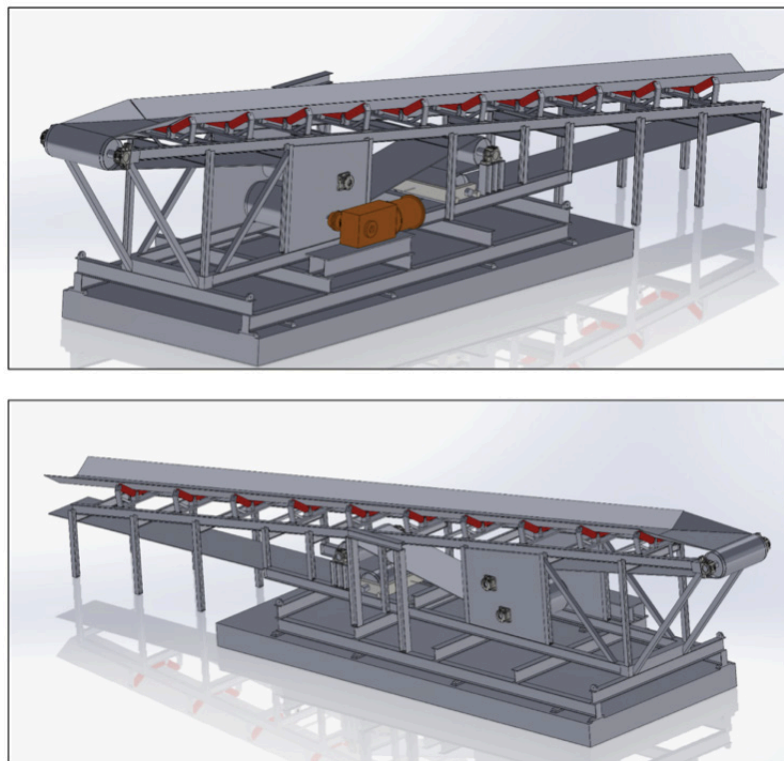
Figure 8 - 3D Model View

It can be seen that the majority of the structure is constructed from I beam section. Because I beam has been used, a modular design was implemented. The modular design was implemented through the following. Firstly, a fully fixed base structure was implemented for the modular design to connect to. It was necessary that the base be fixed as it will have most of the force transferred into it, therefore it must be able to support this. The base of the structure uses the existing concrete footings. The rest of the design was built off the base. To implement the 8 degree incline to the head pulley, the arches were designed at differing lengths with the cross member being angled to accommodate the incline. The gallery section of the overland conveyor was simply supported using I beam arches as well. From the design, it can be seen that two methods were used to support the pulleys. Firstly, on the second bend pulley a platform as built using I beams to mount the bearings. Because of its position in the structure, this was the most elegant solution. The first bend pulley and drive pulley can be seen to be mounted with flange bearings to a sheet metal wall. Furthermore, this sheet wall also acts as a safety barrier to the pulleys and

also as a mounting position for a lubrication station for the system.

It can be seen that the first bend pulley and drive pulley are located at the front end of the system, allowing the clean side of the belt to be taken up by the drive pulley. Furthermore, it can be seen that the take up pulley acts horizontally and as such has been placed on a trolley. This trolley is then connected via a series of pulleys to the take up weight using 14 mm galvanized steel rope. Furthermore, it can be seen that all rollers are at a suitable height above the ground for proper inspection and maintenance procedures to be conducted without the need for raised platforms.

The next stage in the development of the 3D model is a finite element analysis of the structure. To do this, load cases in accordance with the standards review will need to be developed. In undertaking the FEA, finalized sizings of the members used as well as if cross bracing is necessary will be determined.

3 PERFORMANCE ANALYSIS

3.1 POWER CALCULATIONS

3.1.1 STEADY STATE CONDITIONS

Initially the carrying capacity of the belt conveyor must be calculated in order to determine the power required. The carrying capacity of a belt conveyor is carried out as per (PATIL et al., 2015), and is as follows:

$$\dot{m}_s = \rho_b A v k_s \quad (17)$$

Where ρ_b denotes Density of Bulk Material, A is Cross-sectional area, v is Belt velocity and k_s denotes Slope Factor. According to the equations 1 to 6 the following parameters include effective tension (F_e), maximum tension (F_1), minimum tension (F_2), carrier sag tension, return sag tension and motor power can be calculated.

3.1.2 NON-STEADY CONDITIONS

During both the acceleration and deceleration cycles, the transient forces-imposed result in extra stretch not encountered during steady state operation. This may result in early splice failure, excessive take-up travel, and other difficulties. These non-steady conditions including the start-up and coasting of the conveyer must be considered. The non-steady operating conditions are calculated using (GOLKA et al., 2007), in addition with Belt Analyst software. The following outlines the calculations for the start-up time, start-up force and coasting time for normal operating conditions.

The starting time (t_s) is as follows:

$$t_s = \frac{v}{a} \quad (18)$$

Therefore, the starting effective tension (F_{se}) is calculated as follows:

$$F_{se} = F_a + F_e \quad (19)$$

As the motor incorporates a backstop, the coasting time (t_c) is as follows:

$$t_c = (I_d + \left(\frac{I}{\eta}\right))\omega_s/(M_u) \quad (20)$$

Where ω_s is angular velocity of drive pulley, (M_u) is the resistance torque at the motor shaft and I is inertia.

3.2 GEARMOTOR SELECTION

According to the diameter of the drive pulley, and the belt speed, output speed, and the motor required power, a helical-bevel gearmotor specified to be KH167 DRN315L4 is chosen from the selection tables in SEW-EURO Drive Gearmotor catalogue (Gearmotors-6oHz Catalog, 2016). The relevant technical data is listed below in Table 2.

Table 2 - Summary of KH167 DRN315L4 Relevant Technical Data

Motor Power (kW)	Motor Speed (rpm)	Motor Rated Torque (Nm)	Output Speed (rpm)	Output Torque (Nm)	Gearbox Ratio (i)
160	1787	860	88	17300	20.32

3.3 BACKSTOP SELECTION

The purpose of the backstop is to prevent the shaft from rotating in the reverse direction. The selection process is done as per Marland Clutch (MARLAND CLUTCH COMPANY). The low speed backstop BC-18MA with a max bore size of 140 mm is selected as the rated torque exceeds the minimum torque rating. A BCMA Backstop Automatic Grease Lubrication System will be installed to automate the lubrication process.

3.4 PULLEY SIZING

3.4.1 DRIVE AND HEAD PULLEY

The dimensions of the pulley have been designed to be able to withstand the force imparted on them when under maximum operating conditions, the calculations for which can be seen in Section 2.4.1. These calculations shown in Table 3. These initial sizings will be used as a basis for FEA simulations with adjustments to be made accordingly. Furthermore, plate thicknesses will also be sized using FEA simulations. For drive and head pulley, initially a wall thickness of 25 mm will be used and for take-up and snub pulleys, initially a wall thickness of 25 mm will be used with a 75 mm thick plate to be used near the shaft.

Table 3 - Pulley Sizing

Pulley	DIA (mm)	Wall Thickness (mm)	Shaft DIA (mm)
Drive and Head pulley	500	14	Head pulley: 110 Motor coupling: 140 Drive pulley: 135
Take-Up and Snub pulleys	400	14	110

The lagging that is to be used on the drive and head pulley is abrasion resistant quality rubber diamond lagging suggested by (GOLKA et al., 2007). Diamond grooving patterns have been selected as, like car tires, the diamond pattern allows the pulley to still maintain friction with the belt even when wet or dirty. The plain pattern has been selected as it is recommended for take-up and snub pulleys. Because of the environment that the conveyor will be subjected to, this is necessary. The split plumber block type bearing will be used for the head and rear snub pulley whilst the flanged type bearing will be used for the drive and front snub pulley. The materials used for the pulleys are 4140 steel for the shafts and Grade 250 mild steel for the drums.

3.5 IDLER SIZING

The carrier idlers selected were the Lorbrand Series 25 with 6205-2RS bearings with a roller diameter of 127 mm (Figure 9). These 3 trough rollers at a 35 degree angle have a capacity of 208 kg. Table 4 shown the dimension of carrier idlers.
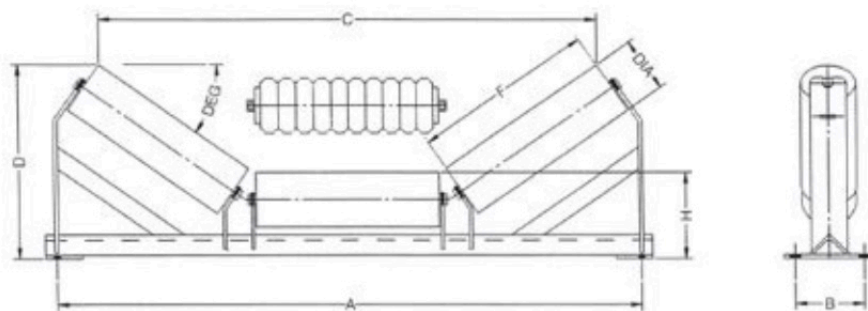
Figure 9 - Carrier Idler Selection

Table 4 - Dimension Description of Figure 6

DEG (∞)	DIA (mm)	A (mm)	B (mm)	C (mm)	D (mm)	F (mm)	H (mm)
35	127	1200	160	1143	350	390	216

The return idlers selected are the Lorbrand Series 25 with 6205-2RS bearings with a diameter of 102 mm (Figure 10). These single roller idlers have a load capacity of 62 kg. The dimension of return idlers shown in table 5.
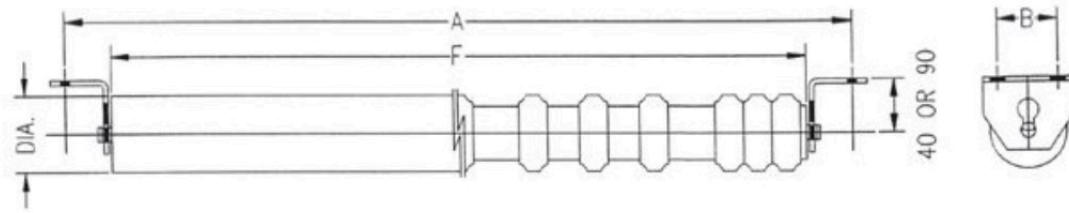
Figure 10 - Return Idler Selection

Table 6 - Dimension Description of Figure 7

DIA (mm)	A (mm)	B (mm)	F (mm)
102	1200	70	1146

4   FINITE ELEMENT ANALYSIS SETUP

4.1   PULLEYS

Pulley models representative of that described in section 2.3 were used as the base model for FEA analysis. This included the pulley and shaft all in one. Firstly, cylindrical supports which allowed radial displacement but not tangential or translational were included on either end of the shaft over an area equal to that of the bearing housings used to model the bearing contact. When examining the FEA results of Lorbrand pulleys, it can be seen that this same method of fixing the shaft was employed (LORBRAND: Conveyor Pulleys, 2019). Next a force equal to double the effective frictions calculated in Section 2.1 for maximum operating conditions was applied to an area equivalent to the contact area of the belt around the pulleys. This force then acted in the direction of the belt. Maximum operating conditions were applied only as they were determined to be the worst out of all the cases studied. Inertial loads were then added. This included an angular velocity equal to 9 rad/s for the drive pulley and 11 rad/s for the take-up and snub pulleys. These angular velocities correspond to the required belt speed of 2.2 m/s. Finally, for the drive pulley only, a moment equal to 17.2 kN.m was applied to the shaft. This moment is equal to the output torque of the selected motor. The model setups for each of the pulleys can be seen in Figure 11.

a

b
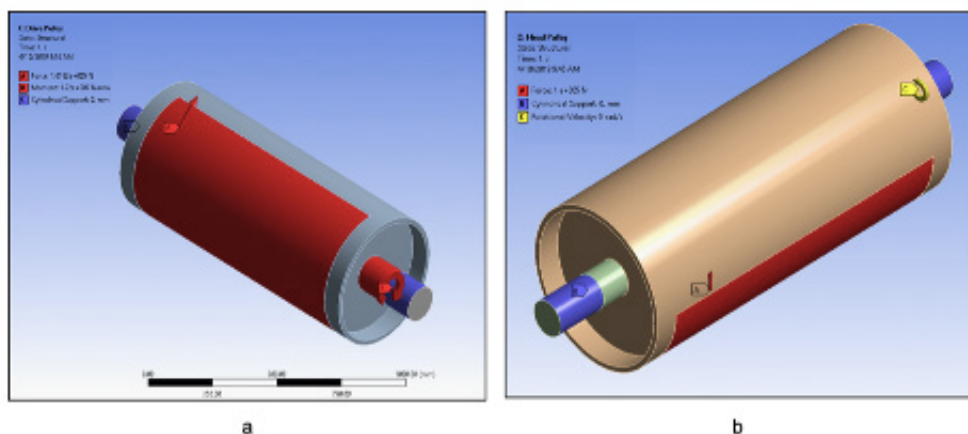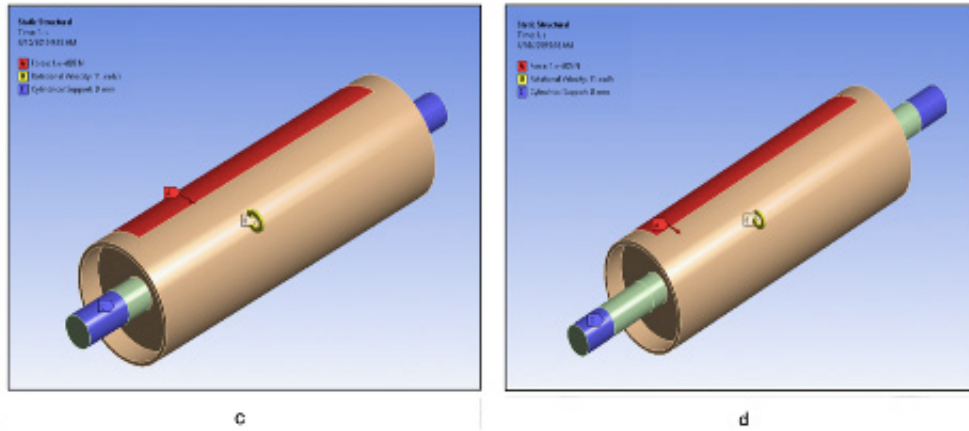
Figure 11 - a) Drive Pulley Model Setup, b) Head Pulley Model Setup, c) Take-Up and Snub

The material used was 4140 steel. It has a tensile yield strength of 665 MPa, an ultimate tensile yield strength of 1000 MPa and a fatigue limit of 250 MPa. Grade 250 mild steel has a yield and ultimate tensile strength of 250 MPa. A tetragonal mesh method was used with refinements placed at the bearing faces and the drum side walls.

4.2 WIND LOADING

Wind loading is an important consideration in the design of the take-up structure and as such must be modelled. In order to set up the wind loading model firstly, the wind pressures acting on the structure had to be determined. The following shows the process following AS 1170.0 and AS 1170.2.

Firstly, the site wind speed $V_{sit,\beta}$ had to be calculated for both SLS and ULS conditions where SLS conditions signify everyday wind speeds and ULS signifies cyclonic wind speeds. The process for determining the SLS wind speed is shown below.

$$V_{sit,\beta} = V_R M_d (M_{z,cat} M_s M_t) \quad (21)$$

Where V_R is the regional gust wind speed, M_d is the wind directional multiplier, $M_{z,cat}$ is the terrain/height multiplier, M_s is the shielding multiplier and M_t is the terrain multiplier.

Pressure is calculated using the following equation:

$$p = (0.5\rho_{air})\left(V_{sit,\beta}\right)^2 C_{fig} C_{dyn} \quad (22)$$

Where ρ_{air} is the density of air taken to be 1.20 kg/m3, C_{fig} is the aerodynamic shape factor based on the members and C_{dyn} is the dynamic response factor which is given as 1.0. C_{fig} is dependent on the type of member and its orientation relative to the wind direction.

The setup of the ULS loadings can be seen in Figure 12, with the only difference being observed with the SLS conditions being the magnitude of the pressures applied.
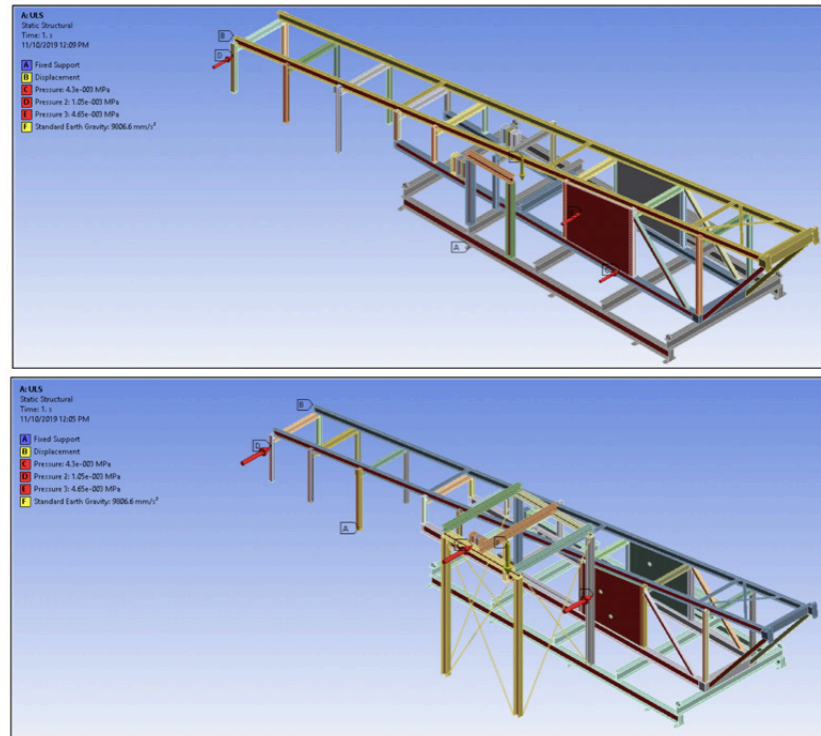
Figure 12 - ULS Model Setup, design 1 and design 2

The mesh used was a default mesh and using the structural error tool, the mesh was refined in places of both high error and high stress. It was detected that the places of high error were in places of little to no stress which validates the model set up approach. Grade 250 mild steel used for the structure of the system included sections of I beam, hollow section and plate. It has a yield and ultimate tensile strength of 250 MPa.

4.3   SKID FRAME

Two Load cases were conducted and analyzed using Autodesk Inventor. The conveyor was imported into Autodesk and all unnecessary components were removed leaving the frame. The idlers were partially removed leaving only the footprint of where they were to make force application more accurate. To begin fixed constraints were added to all the attachment points where the conveyor is attached to the concrete block or an assumed fixing point at the bottom of the structure as shown in Figure 13.
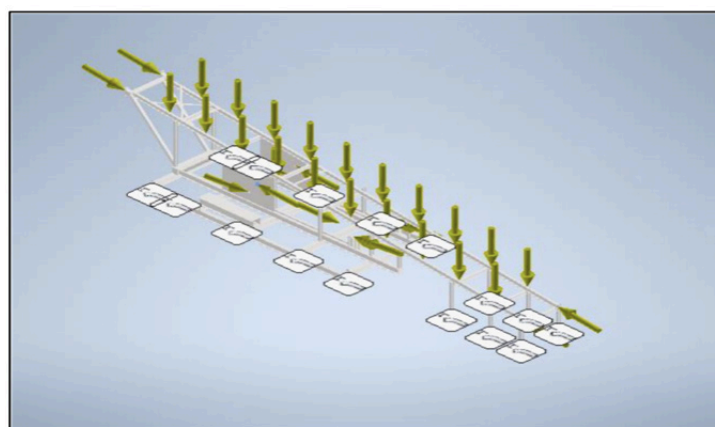
Figure 13 - Applied Loads

Next the gravity force was applied to take into consideration the weight of each member of the frame. A weight force was added to the idler footprints left to model the weight of the sand being transported. The bearing loads were applied through the circular supports within the metal plates on either side of the frame. A perpendicular tension force was applied to the ends of the frame to simulate the belt compressing the frame. The final force applied to the frame was that of the force acting through the cross-bracing member under the strain of the gravity take ups tension. All forces are shown in Figure 14.
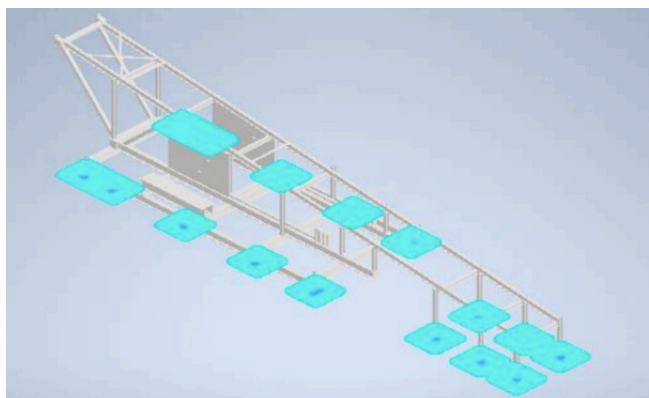
Figure 14 - Fixed Supports

Grade 250 mild steel was used and it has a yield and ultimate tensile strength of 250 MPa. The type of mesh used was curved with the average element size used for meshing was 0.05 mm and a minimum element size of 0.1 mm. The turn angle used was the default setting of 60°.

4.4 TAKE-UP WEIGHT STRUCTURE

The take-up weight structure was simply modelled using fixed supports and a point load. It was modelled separately to the rest of the skid frame as to allow for more accurate results. The model was setup as follows. Firstly, fixed supports were introduced at the base of each of the vertical supports. As two of the vertical supports will be concreted into footings in the ground, and the other two are connected via welds to the base frame, which is ion turn fixed to cement footings, the use of this type of boundary condition was rendered plausible. Secondly, as the weight will be supported from the center of the middle cross member, a single point load was added to act at this position. The magnitude of this point load was equal to that of the weight of the counterweight. The ANSYS setup of the model can be observed in Figure 15.
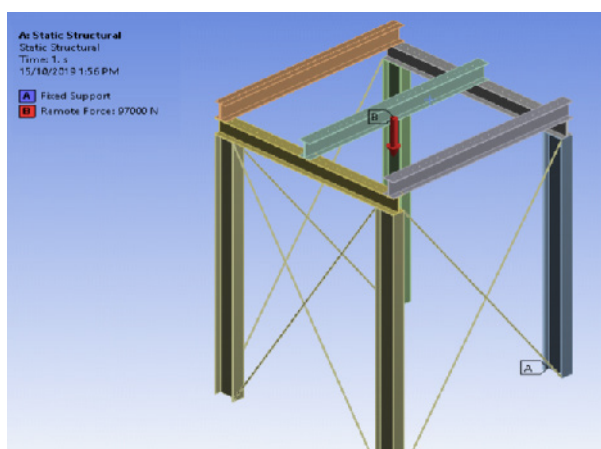

Figure 15 - Take-Up Weight Model Setup

4.5 TAKE-UP TROLLEY

The take-up trolley was simply modelled using a force and fixed supports. Fixed supports were used at the bearing positions. The absolute maximum stress that would ever occur in the trolley under any circumstance was modelled. A force equivalent to the take-up weight was placed in the appropriate position to model the weight pulling on the trolley. The model setup can be seen in Figure 16.
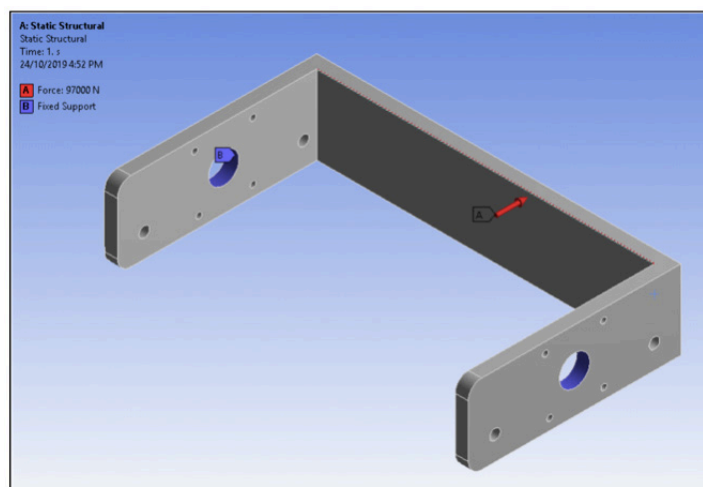

Figure 16 - Take-Up Trolley Model Setup

The materials used to construct the take-up trolley was 50 mm Grade 250 mild steel plate. A default 7 mm mesh size was used for the entirety of the structure with refinements 2 mm edge refinements made along the corners of the structure. This gave an insignificant structural error within the structure, hence validating the model.

5 FINITE ELEMENT ANALYSIS RESULTS

5.1 PULLEYS

5.1.1 DRIVE PULLEY

From observing Figure 17, it can be seen that the maximum stress within the pulley assembly is 148.24 MPa. This occurs on the shaft on the edge of the bearing support. Furthermore, a stress profile has developed in the pulley wall which is what is expected from previous results. When closely examining the stress profile at the maximum position, it can be seen that the maximum actually occurs at the intersections of the nodes of the elements. From this, it can be determined that these stresses are anomalies because of the mesh used. It must be noted that the mesh chosen was the best mesh that could be applied for the licensing limitations of the ANSYS software. With this in mind, the actual stress that can be observed would more likely be in the range of approximately 100 MPa, or the stress observed surrounding the maximum peaks. As 4140-steel was used for that shaft, this gives a static safety factor of 6.65, where 665 MPa is the yield strength of the material. For the pulley itself, standard mild steel was used with a yield strength of 250 MPa. The maximum stress observed in the pulley is approximately 45 MPa, giving a static safety factor of 5.55. Hence the drive pulley will not fail by yield.
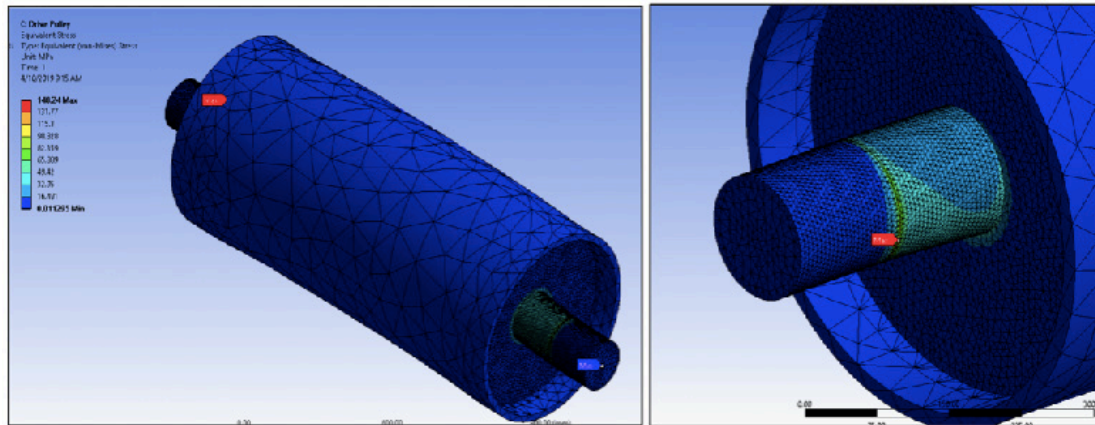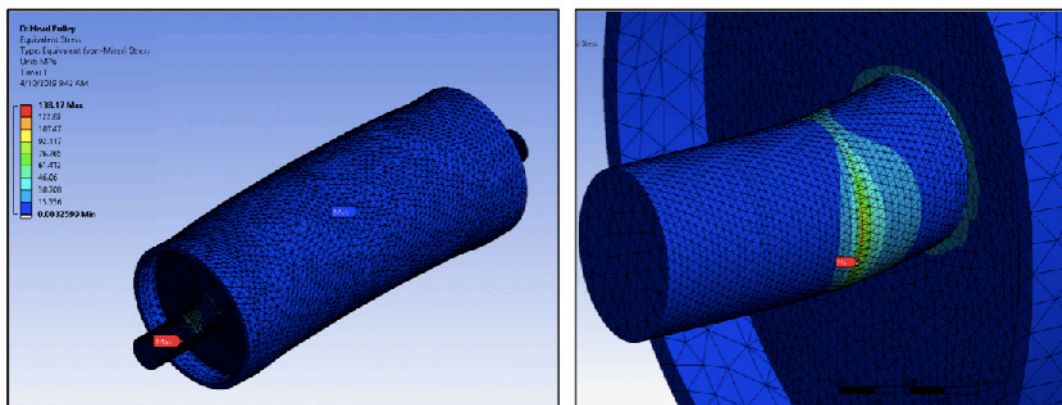
Figure 17 - Drive Pulley Stress Profile

As these components of the entire system are subjected to fatigue loading, a fatigue analysis was undertaken. To undertake the fatigue analysis the conditions used were fully reversed loading with a fatigue factor of 0.75. Moreover, the Goodman's method was used. As the loading is fully reversed, the mean stress of the system is equal to zero. Therefore, Goodman's equation can be defined as:

$$\frac{\sigma_a}{\sigma_e} = \frac{1}{N} \quad (23)$$

Where σ_a is the alternating stress equal to the maximum stress observed in the system for fully reversed loading and σ_e is equal to the fatigue factor multiplied by the fatigue limit of 4140 steel which is equal to 0.75 x 250 MPa = 187.5 MPa. Therefore, the safety factor of the system is equal to:

$$N = \frac{187.5}{100} = 1.875 \quad (24)$$

This safety factor signifies infinite life of the system which meets the requirements.

When examining the deformation profile (Figure 18), the profile itself can be seen to follow what is expected by results of similar systems. The maximum deformation occurs at the center of the drum where the load is applied and is equivalent to 0.188 mm. It must be noted that interior reinforcement as well as increasing the shell thickness to 17 mm from the original 14 mm was added to the drum for the purpose of reducing the deformation observed.
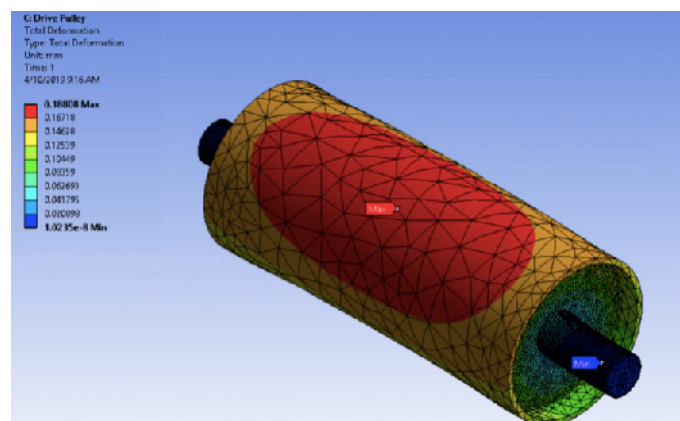
Figure 18 - Drive Pulley Deformation Profile

5.1.2 HEAD PULLEY

Similar to what is observed in the drive pulley, the maximum stress is found to occur on the shaft on the edge of the bearing mounting position (Figure 19). The maximum value observed is 138.17 MPa but again, similar to the head pulley this number occurs on the corner of the nodes of the elements leading to anomalies. As such, it is expected that the maximum stress is more resemblant of the encompassing stress profile which can be observed to be approximately 95 MPa. Once again, as this stress occurs in the 4140-steel shaft, a static safety factor of 7. The maximum stress observed in the pulley drum is approximately 35 MPa. This gives a static safety factor of 7.14. Hence the head pulley will not fail by yield.

Figure 19 - Head Pulley Stress Profile

Once again, as the pulley is subjected to fatigue loading, a fatigue analysis was conducted. The same parameters as was used in the fatigue analysis of the drive pulley were also implemented here. This gave a safety factor equivalent to:

$$N = \frac{187.5}{95} = 1.974 \qquad (25)$$

This gives infinite life, once again meeting the client's requirements.

When examining the deformation profile (Figure 20), the profile itself can be seen to follow what is expected by results of similar systems. The maximum deformation occurs at the center of the drum where the load is applied and is equivalent to 0.0665 mm. It must be noted that interior reinforcement was added to the drum for the purpose of reducing the deformation observed.
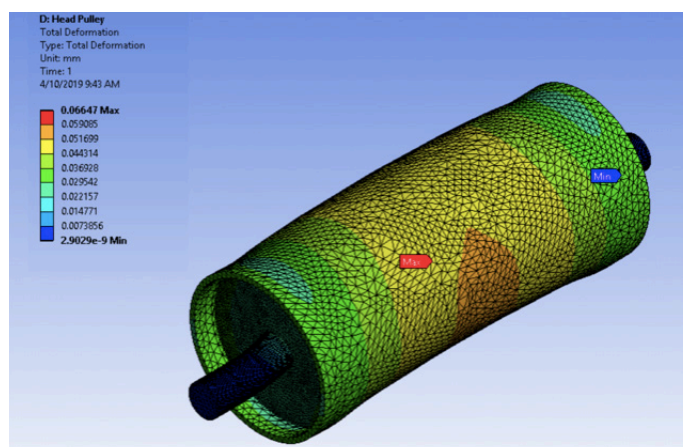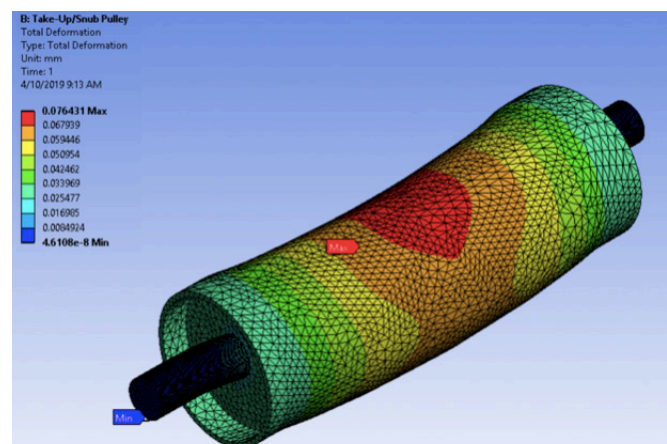

Figure 20 - Head Pulley Deformation Profile

5.1.3 TAKE-UP AND SNUB PULLEY

Once again, as observed in the previous two analyzed pulleys, the maximum stress in the take-up and snub pulley is observed to occur on the shaft at the edge of the bearing housing (Figure 21). This value is observed to be 109.76 MPa, however, similar to the previous, this occurs on the intersection of the nodes at the corner of the elements. With this in mind, the maximum stress is more appropriately valued at approximately 85 MPa, which is the maximum stress of the surrounding profile. When observing the drum, a maximum stress of approximately 30 MPa is observed. This gives a static safety factor of 7.82 for the shaft and 8.33 for the drum, validating that the system will not fail by yield.
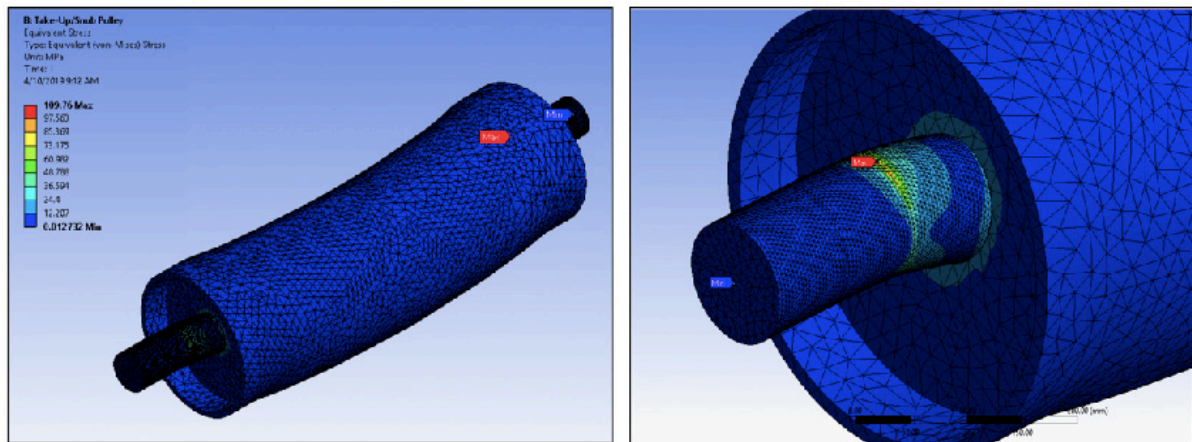
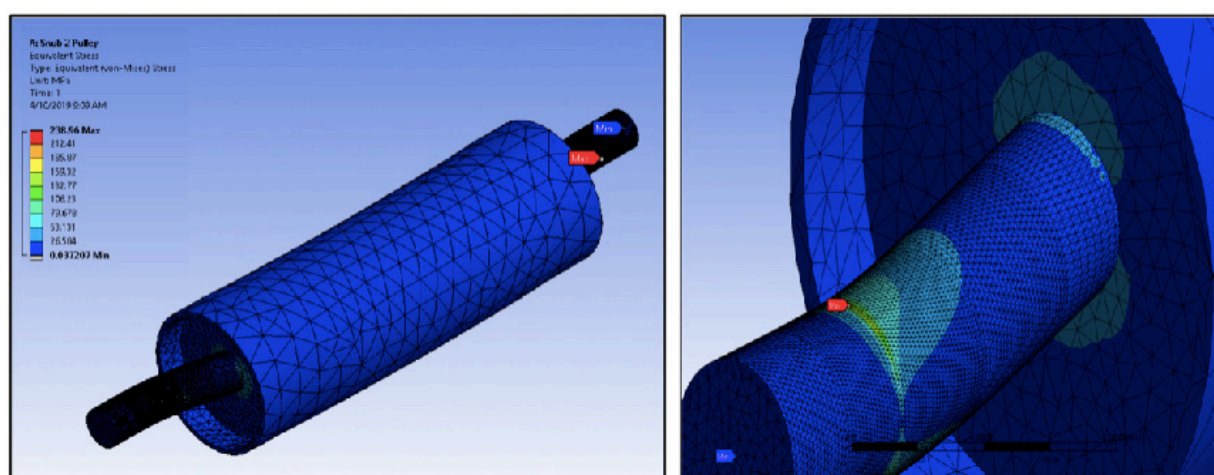**Figure 21** - Take-Up and Snub Pulley Stress Profile

Once again, as the pulley is subjected to fatigue loading, a fatigue analysis was conducted using the same parameters as previous. This gave a safety factor of:

$$N = \frac{187.5}{85} = 2.206 \quad (26)$$

This equates to infinite life, meeting the requirements set forth by the clients.

When examining the deformation profile (Figure 22), the profile itself can be seen to follow what is expected by results of similar systems. The maximum deformation occurs at the center of the drum where the load is applied and is equivalent to 0.0764 mm. It must be noted that interior reinforcement was added to the drum for the purpose of reducing the deformation observed.
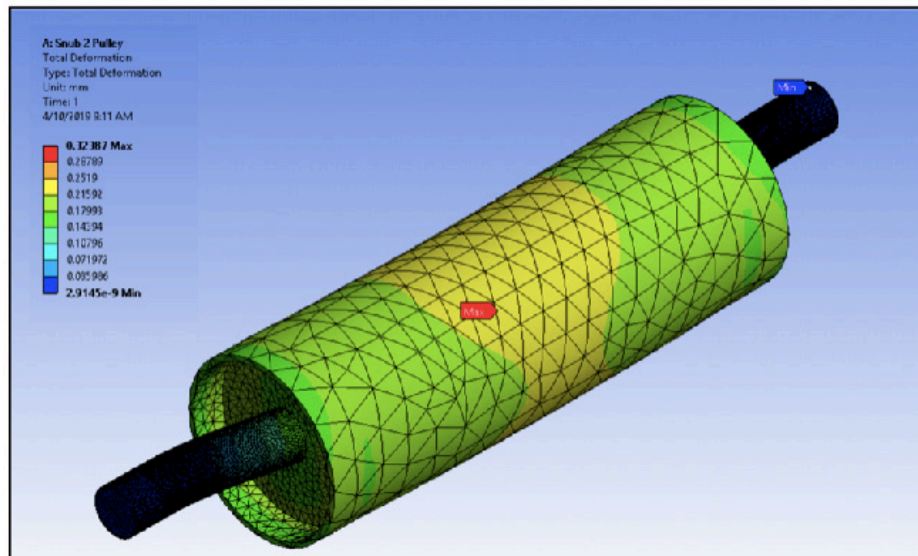

Figure 22 - Take-Up and Snub Pulley Deformation Profile

5.1.4 DRIVE SNUB PULLEY

The maximum stress observed in the drive snub pulley is 238.96 MPa, which can be seen to occur in the same position, i.e. on the shaft at the edge of the bearing housing, as the other pulleys analyzed (Figure 23). The reason for the large difference between this pulley and the others is a direct result of the shaft length. Because of the position of the pulley in the system, a shaft length of 1850 mm was required, which is longer than the 1600 mm shafts used for the other pulleys. Because of this, a larger moment is generated in the shaft hence giving the higher stress observed. However, like the other pulleys, this stress occurs at the corner of a node intersection giving results that are higher than what would be deemed accurate. As a result, the stress more accurate of what is occurring can be defined as 130 MPa, or the maximum stress of the surrounding profile. In the pulley drum, the maximum observed stress is 80 MPa. With these values, a static safety factor of 5.12 is observed in the shaft and 3.125 is observed in the pulley drum. This validates that the system will not fail by yield.

Figure 23 - Drive Snub Pulley Stress Profile

Once again, as the pulley is subjected to fatigue loading, a fatigue analysis was conducted using the same parameters as previous. This gave a safety factor of:

$$N = \frac{187.5}{130} = 1.442 \quad (27)$$

This equates to infinite life, meeting the requirements set forth by the clients.

When examining the deformation profile (Figure 24), the profile itself can be seen to follow what is expected by results of similar systems. The maximum deformation occurs at the center of the drum where the load is applied and is equivalent to 0.3239 mm. It must be noted that interior reinforcement was added to the drum for the purpose of reducing the deformation observed.

Figure 24 - Drive Snub Pulley Deformation Profile

5.1.5   SUMMARY

The results of the FEA justify the theoretical calculations conducted in the performance analysis. Other than the small adjustment needed in increasing the wall thickness of the drive pulley, all other calculations for the pulley sizing met the specification of steel as per AS 4100 and AS 3990 from a strength and serviceability from a static standpoint. The pulleys were also analyzed under fatigue loading and again, met the strength and serviceability requirements over the agreed upon life of the skid frame. It must be noted that the results displayed are full maximum loading conditions as this through the FE analysis was deemed to impart the worst stresses and deformation into the pulleys. Furthermore, the analysis of these pulleys are validated by the calculations undertaken in Section 2.4.1 of the report.

5.2   WIND LOADING

5.2.1   SLS

5.2.1.1   FIRST DESIGN ITERATION

The first iteration of the take-up design under SLS wind loading yielded a maximum von mises stress of 53.724 MPa in the front footing of the structure as observed in Figure 25. This value is well below the yield stress of the material used, 250 MPa, and as such will not fail by yield with a static safety factor of 4.65 observed. As this is analysis was for wind loading conditions, fatigue was not considered for this model. Furthermore, as this is loading scenario is for day to day wind loading conditions, the main point of concern is with the deformation of the system. As can be seen, the maximum deformation observed is 7.6843 mm (Figure 26). This value is observed in the take-up weight structure. This value is considerably high for the day to day loadings of the system and as such should be adjusted in the future design to reduce the deformation observed.
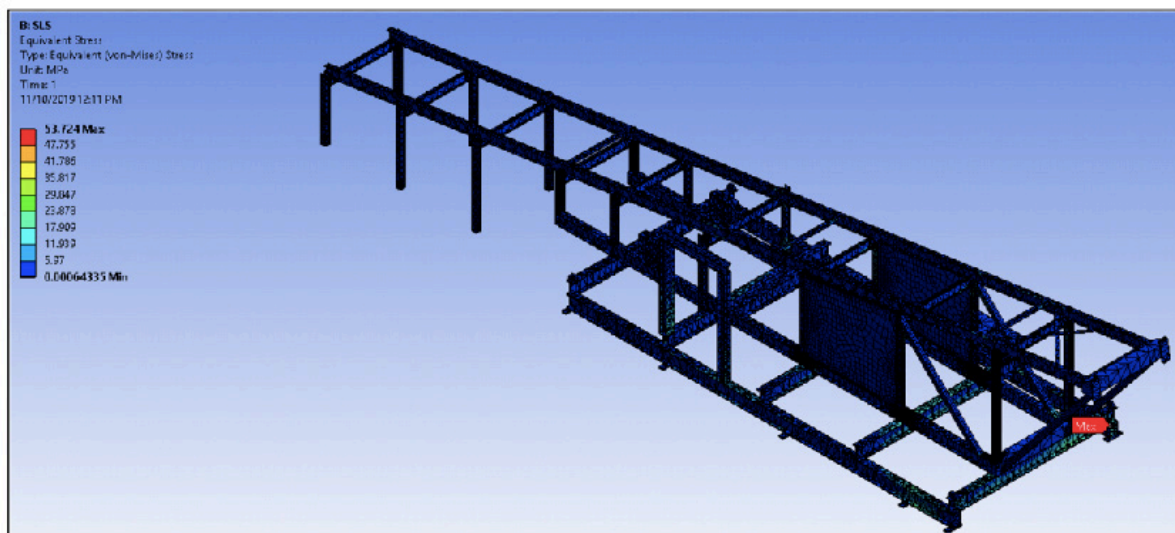
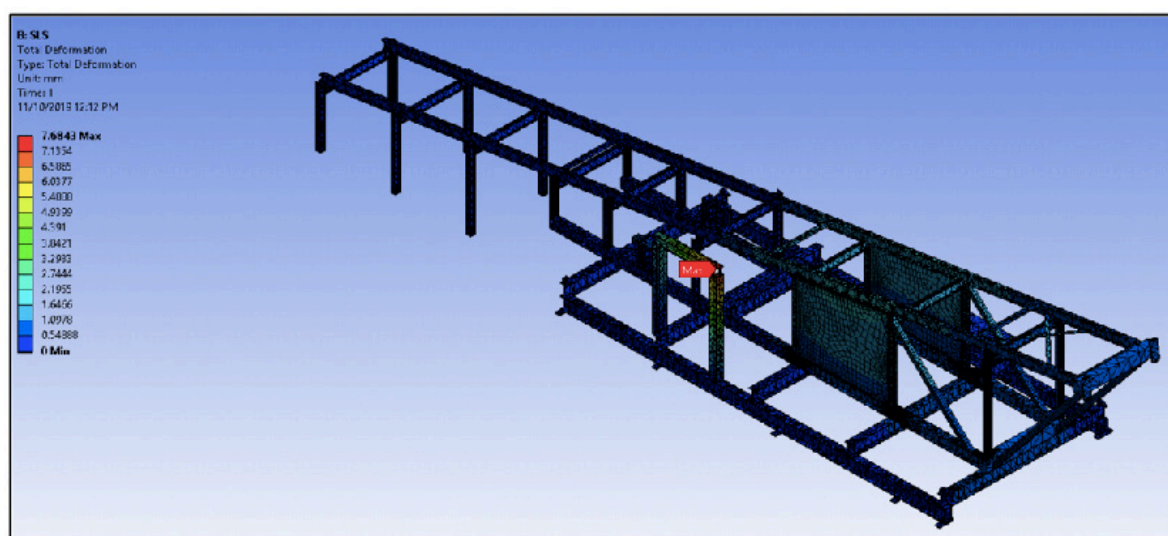**Figure 25** - SLS Stress Profile - First Design

Figure 26 - SLS Deformation Profile - First Design

5.2.1.2 SECOND DESIGN ITERATION

In the second design iteration, the size of the base members was increased as well as including a four-post take-up weight structure. In doing this, two things were achieved, firstly, the maximum stress was increased to 59.496 MPa (Figure 27). The location of this was again in the front footing of the structure. Although the stress increased, the benefit in the positioning of the maximum stress is that it is transferred straight into the concrete slab and out of the take-up structure. Furthermore, the maximum stress is still well below the yield limit of the steel used giving a static safety factor of 4.2. However, as previous, for SLS loading, the main consideration is the deformation of the structure (Figure 28). The deformation was reduced to 2.2631 mm and moved into the pulley wall support. For SLS loading, 2.2631 mm over the 2.5 m span of the wall support is negligible and as such deemed to meet the specifications.
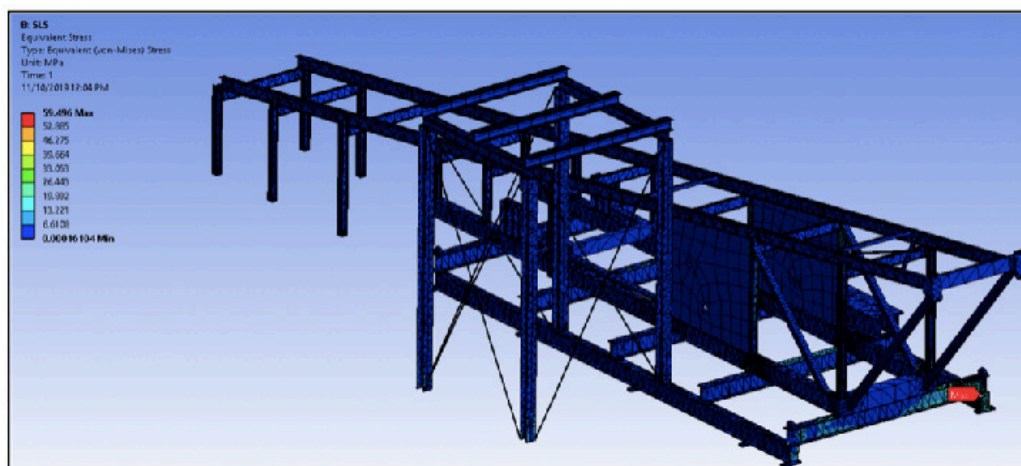
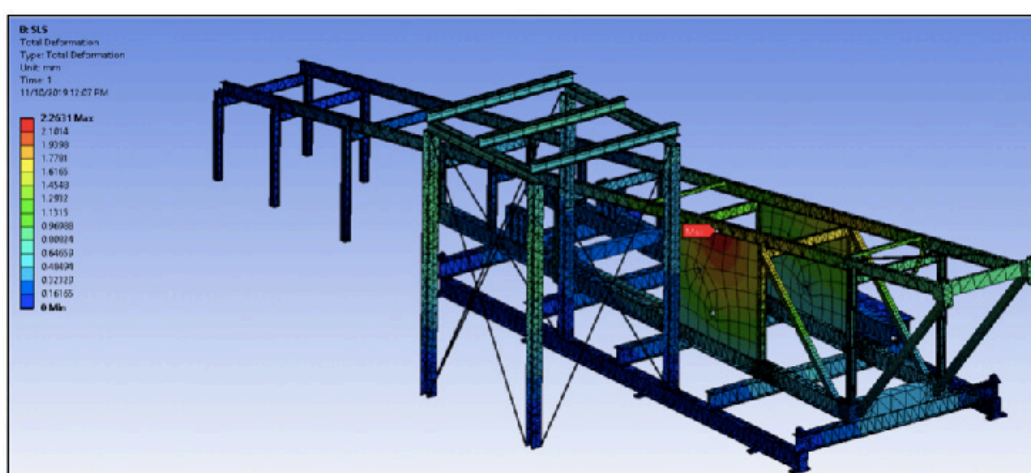**Figure 27** - SLS Stress Profile - Second Iteration

Figure 28 - SLS Deformation Profile - Second Iteration

5.2.2 ULS

5.2.2.1 FIRST DESIGN ITERATION

Under ULS wind conditions, the maximum stress observed in the initial design of the take-up system is 79.324 MPa, which occurs in the base structure of the frame below the pulley wall support (Figure 29). Although well below the yield strength of the material giving a safety factor of 3.15, the positioning of the stress is not ideal. As for ULS wind loading conditions, stress becomes the critical criteria in the suitability of the design, the positioning of the maximum stress is highly important. Because of this, the size of the base members was increased in the second design iteration. Furthermore, the maximum deformation in the structure was observed to be 14.171 mm in the corner of the take-up weight structure (Figure 30). Although deformation is not the critical criteria for the design for ULS loading conditions, the deformation observed is too high and was hence remediated in the second design iteration.
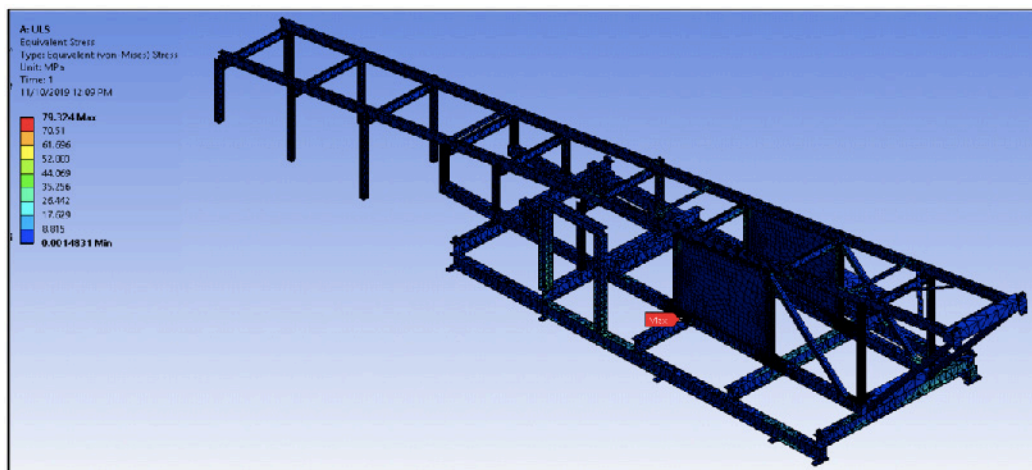
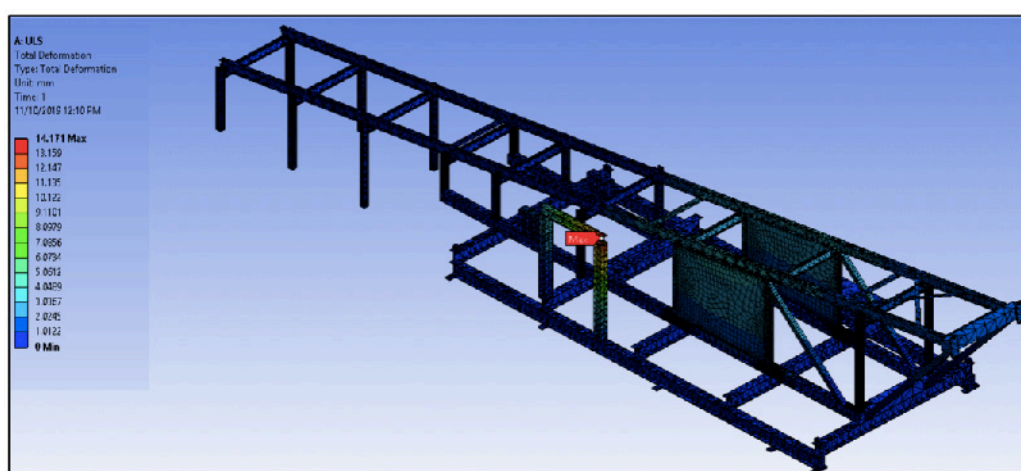**Figure 29** - ULS Stress Profile - First Iteration

Figure 30 - ULS Deformation Profile - First Iteration

5.2.2.2 SECOND DESIGN ITERATION

In the second design iteration, three outcomes can be observed. Firstly, the maximum von mises stress was found to be reduced by approximately 13 MPa to 66.731 MPa (Figure 31). This gives a static safety factor of 3.75, indicating that the system will not fail via yield. Secondly, the position of the maximum stress has been shifted to the front footing of the structure. Once again, this is ideal as the maximum stress can be transferred out of the structure into the concrete slab. As for ULS loading, stress in the structure becomes the important criteria, reducing the maximum von mises stress and shifting it to a more ideal location in the footing from the previous design shows how the new design has improved. Lastly, it can also be seen that the deformation has significantly reduced by approximately 10 mm to 4.1993 mm (Figure 32). Although, deformation isn't as important a criterion as stress under ULS conditions, such a reduction to a reasonable deformation gives further confidence in the design.
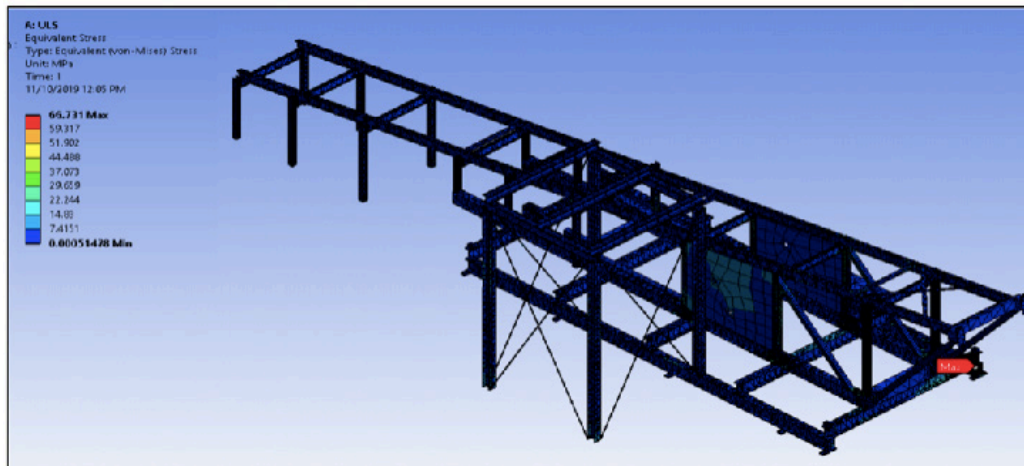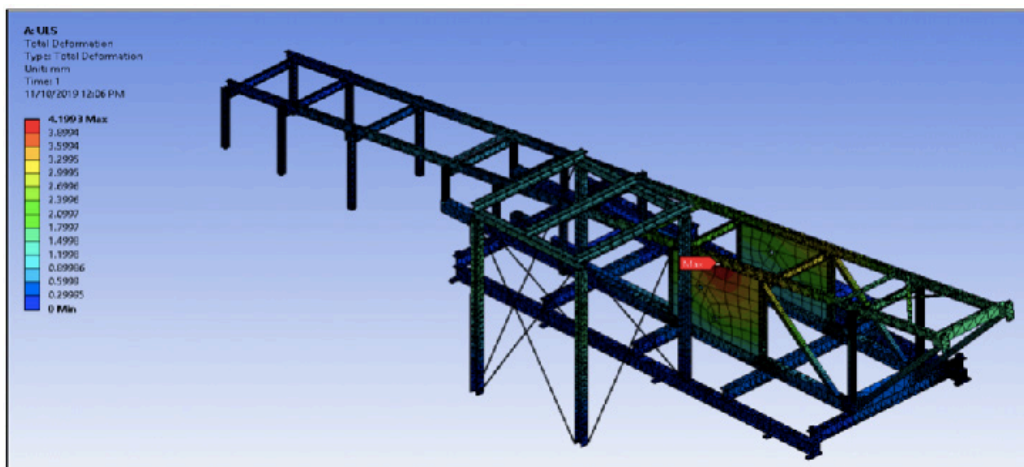
Figure 31 - ULS Stress Profile - Second Iteration

Figure 32 - ULS Deformation Profile - Second Iteration

5.3   SKID FRAME

5.3.1   FIRST DESIGN ITERATION

When analyzing the results of the FEA undertaken on the skid frame, it can be seen that, for the first design, the maximum von-mises stress is equivalent to 568.2 MPa (Figure 33). This value occurs in the cross member that is attached to the take-up pulley. Obviously, this stress is well above the yield strength of the material at 250 MPa hence indicating that the structure will fail by yield. The reason for this high stress is mainly due to the member type used and how the force would subsequently be needed to be applied. An I beam section was used for this member with the force applied perpendicular to the web. In this loading scenario, I beams are suboptimal for handling such a large bending moment due to their moment of inertia in this orientation. Ideally, the I beam should only be subjected to bending when the force is applied perpendicular to the flange. This was not the case for this scenario and a failed system ultimately ensued. Because this failure occurred under maximum conditions, it was deemed unnecessary to continue analysis with the normal operating conditions loading scenario.
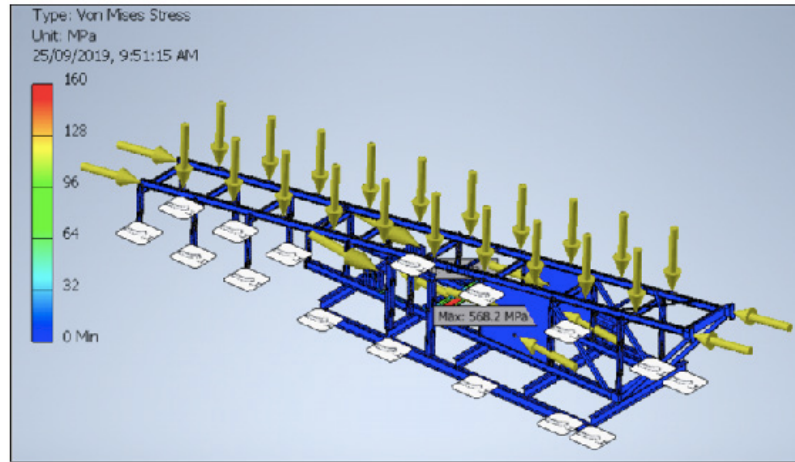
Figure 33 - Skid Frame Stress Profile - First Design

The maximum deformation observed when analyzing the structure was found to be 23.07 mm which once again occurred in the cross member that attached to the take-up pulley (Figure 34). As this cross member was only 1600 mm long, a deformation of 23.07 mm is unacceptable. The reasons for the high value observed is the same as explained previously, i.e. a result of the I beam not performing well in bending under the applied force orientation. This issue was addresses in the next design iteration.
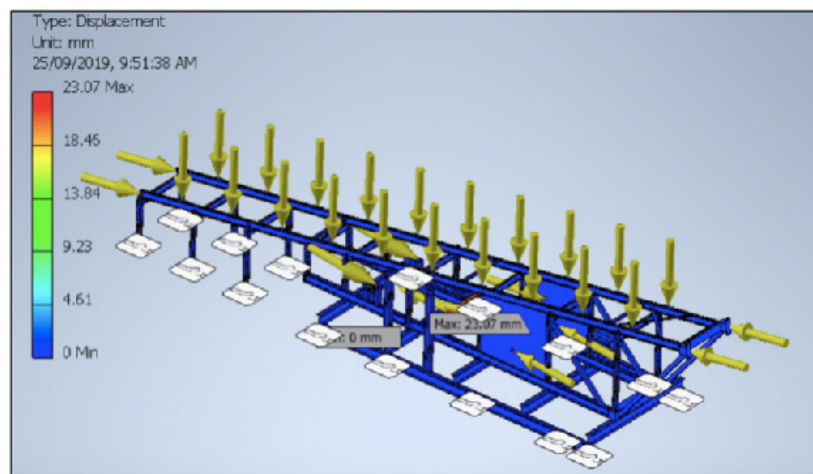

Figure 34 - Skid Frame Deformation Profile - First Design

5.3.2 SECOND DESIGN ITERATION

For the second design iteration, the problematic I beam section cross member was replaced with a rectangular hollow section (RHS) member. In doing this a member more able to handle bending in the designed orientation as a consequence of its moment of inertia was introduced. Furthermore, this design change also moved the location of the maximum stress to from the cross section member to the snub pulley bearing (Figure 35 and Figure 36). By doing this, the stress can be transferred straight into the base frame and into the cement footings, which is idea. The maximum stress that was identified under maximum loading conditions was found to be 217.177 MPa (Figure 36). Although this is close to the material yield strength of 250 MPa, it can still be seen that the system will not fail be yield giving a static safety factor of 1.15. Furthermore, this is for maximum operating conditions. It is expected that maximum operating conditions will

not frequently occur and as such normal operating conditions was analyzed. Under normal operating conditions the maximum stress was found to be 72.36 MPa (Figure 35). This gives a static safety factor of 3.455. When comparing the normal operating conditions to the maximum operating conditions it can be seen that both pass the yield strength assessment with the normal operating conditions falling well within the limits. Because of this, it was deemed unnecessary to further refine the structure for maximum operating conditions. It was decided that because the structure is static, a fatigue analysis was not necessary.
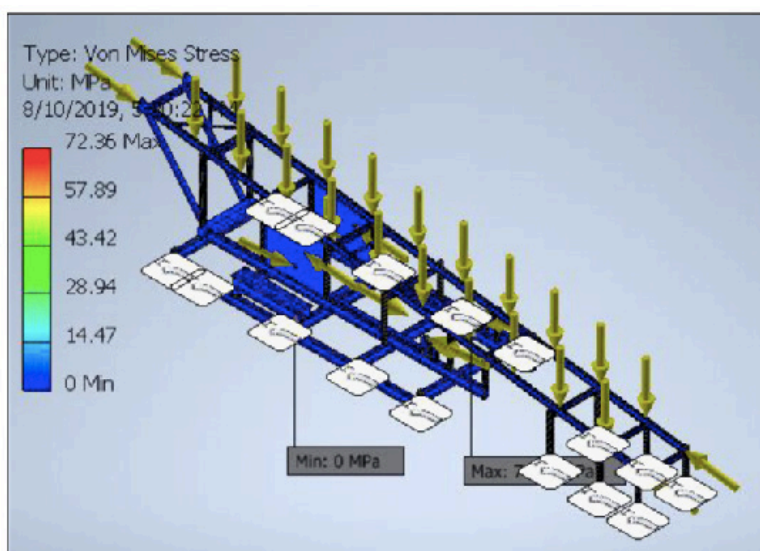

Figure 35 - Skid Frame Stress Profile - Second Design, Normal Operating Conditions
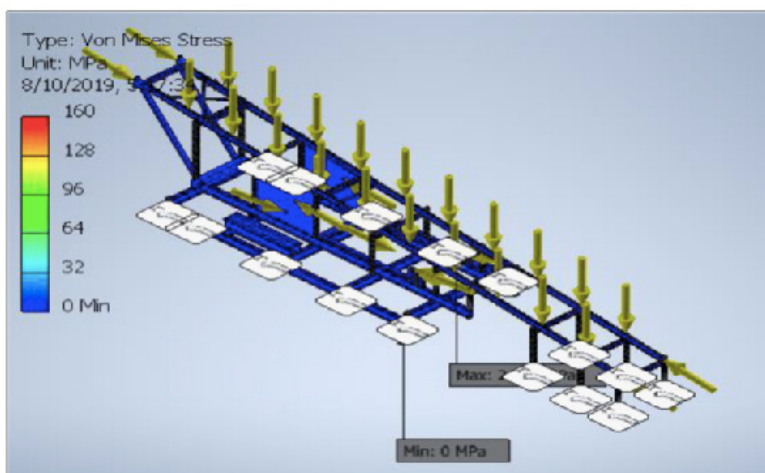

Figure 36 - Skid Frame Stress Profile - Second Design, Maximum Operating Conditions

When the deformation profile of the skid frame is observed, it can be seen that the maximum deformation is 1.437 mm for normal operating conditions and 1.493 mm for maximum operating conditions (Figure 37 and Figure 38 respectively). Both these instances occur in the cross bracing behind the head pulley. This small deformation is acceptable in such a large structure. The deformation is then spread through the head pulley support structure. From these observations it can be seen that no extra support will be necessary to reduce the deformation in the structure.
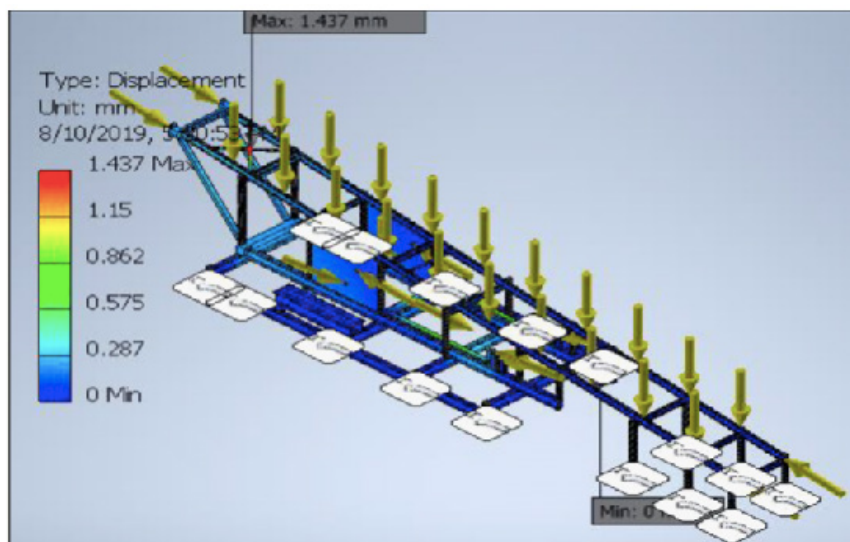
Figure 37 - Skid Frame Deformation Profile - Second Design, Normal Operating Conditions
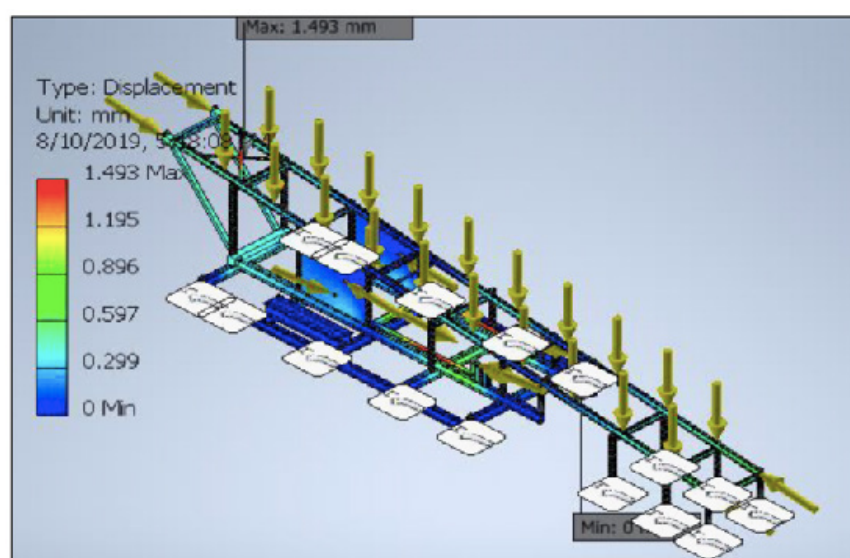

Figure 38 - Skid Frame Deformation Profile - Second Design, Maximum Operating Conditions

5.4 TAKE-UP TOWER

When analyzing the stress profile in Figure 39, it can be observed that the maximum von mises strength present is 99.848 MPa, which occurs at the connection between the middle cross members to the outer cross member. The remainder of the stress is then distributed through the middle cross member and to the sides of the connection with the outer cross member. When comparing the maximum stress to the yield strength of the material, a static safety factor of 2.5 is observed. This indicates that the structure will not fail by yield. As this part of the structure is only subjected to static loading, a fatigue analysis was not conducted. Therefore, with the finding that the system will not fail by yield, it can be seen that the system meets the client's requests.
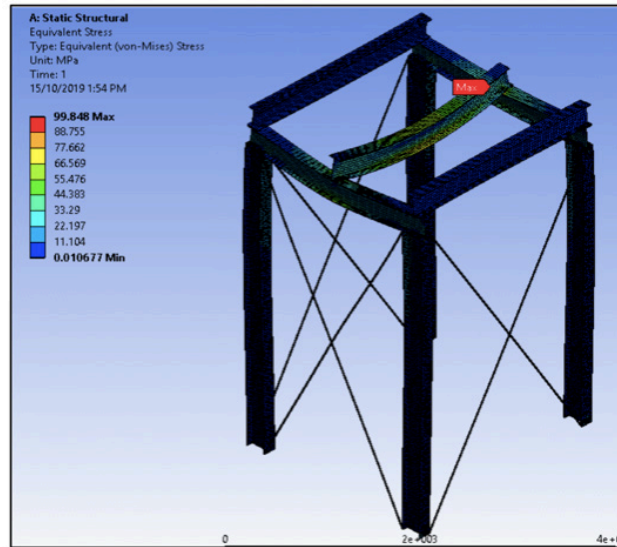
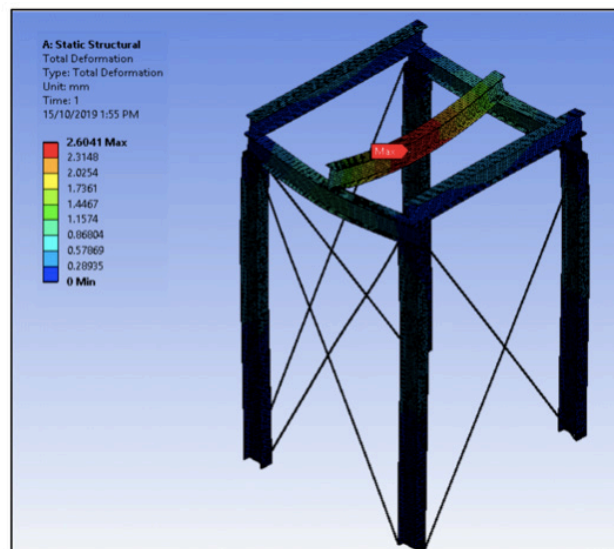**Figure 39** - Take-Up Weight Structure Stress Profile

Figure 40 - Take-Up Weight Structure Deformation Profile

5.5 TAKE-UP TROLLEY

When analyzing the stress profile of the take-up trolley (Figure 41) a maximum von mises stress of 237.7 MPa is observed in the corner of the frame. This is below the yield strength of the material (250 MPa). However, upon closer observation it can be seen that due to the mesh quality, this value is actually an anomaly. It can be seen that the maximum value occurs at the intersection of the nodes. Therefore, the maximum stress is more likely to be that of the surrounding profile, i.e. approximately 172 MPa. This value gives a static safety factor of 1.45, indicating that the structure will not fail by yield.
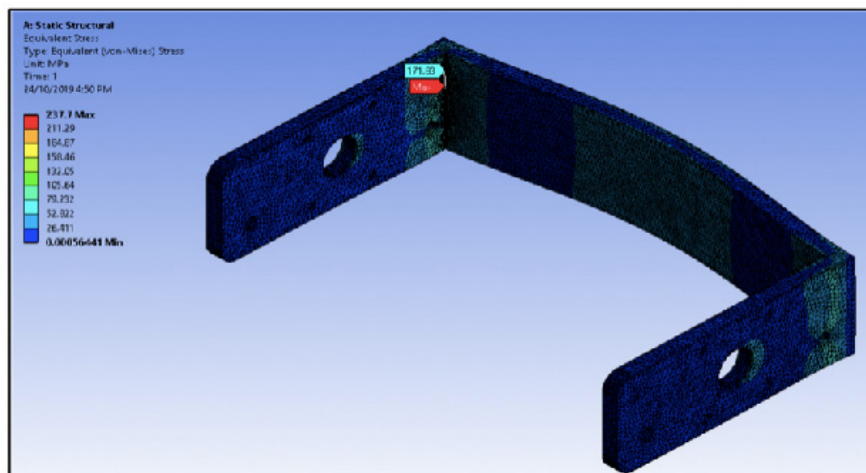
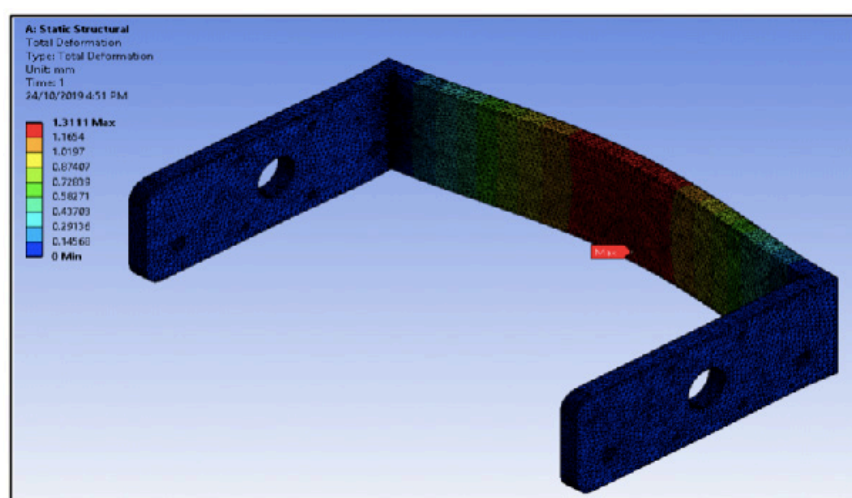**Figure 41** - Take-Up Trolley Stress Profile

Figure 42 - Take-Up Trolley Deformation Profile

6   CONCLUSIONS

In this report, a design proposal for the head end skid frame of an 800 m conveyor covering the drive system, conveyor tension take-up method and ancillary structures/components, structural members for transition section of the conveyor and bend pulleys was completed. The proposed design complies with the requirements set by Rockfield Technologies and satisfies the client's objective of increasing the production.

In the concept development preliminary specifications for the drive system were completed through analytical calculations of the drive capacity and belt tensions. Four unique tensioner arrangements were compared using a decision matrix. Design 4 consisting of head pulley, a drive pulley, two bend pulleys and a horizontally aligned take-up pulley was selected, scoring highest in criteria based on the client's input, which included maintainability, constructability, tensioner arrangement and safety. This was followed by the sizing of the relevant pulley, idlers and bearings. An in-depth material selection for the structural members, considering workability, manufacturability, weldability, machinability, corrosion resistance, physical and mechanical properties, identified that high carbon steel should be used for the skid frame.

As structural members are at high risk to corrosion due to the coastal location, anti-corrosion paint will be implemented as a corrosion protection measure. A performance analysis was

conducted, detailing the analysis of the belt and drive system for the normal and maximum conditions.

Furthermore, the non-steady state conditions were considered with the start-up time, start-up force and coasting time for normal operating conditions calculated. Using these calculations, a gearmotor and backstop were selected. Finite element analysis was conducted on the pulleys, skid frame, take-up weight structure, and take-up trolley. Additionally, a wind loading analysis of the skid frame was conducted. With the exception for a small change in wall thickness of the pulleys, the FEA results on the pulleys justified with the theoretical calculations outlined in the performance analysis. Utilizing FEA and wind loading of the skid frame, refinements to the design were performed in iterations.

The results for the skid-frame under normal operating conditions and maximum operating conditions determined the strength to fall well within the limits of the yield strength. FEA of the take-up structure and take-up trolley showed that they will not fail through yield. Therefore, the overall design will operate with the required strength and serviceability as outlined in AS 4100 and AS 3990 for the agreed upon system lifetime under normal and maximum operating conditions, as well as start-up and shutdown conditions.

INVESTIGAÇÃO DE PROJETO DE ESTRUTURA DE RECOLHIMENTO SOB CONDIÇÕES ESTÁVEIS E NÃO ESTÁVEIS

RESUMO: Este documento deve ser usado como um relatório de progresso de um projeto potencial para uma estrutura deslizante de recolhimento por gravidade. Como resultado, uma nova estrutura deslizante de recolhimento de gravidade é necessária. Para obter o melhor desenho possível para a estrutura de recepção, ela foi separada em quatro fases. A fase um incluiu o desenvolvimento do conceito de design. Verificou-se que o motor deve ser capaz de lidar com 132,3 kW de potência quando a correia estiver totalmente inundada. Fase dois, o material foi selecionado para a construção. A fase três foi a análise de desempenho do projeto. Nesta fase, cálculos que justificam as decisões de projeto, incluindo a capacidade do transportador em condições normais e máximas, bem como as condições de inicialização e desligamento e uma análise das forças de tração da correia em condições estáveis e não-estáveis. O sistema de acionamento também foi analisado para determinar as forças resistivas e a potência subsequente necessária para operar o sistema. Além disso, foi realizada a análise do projeto do acionamento, polias e rolamentos. A fase quatro foi a análise FE do sistema. Isso incluiu uma análise estática na estrutura, incluindo a estrutura de deslizamento e do peso de levantamento, e uma análise de fadiga nas polias. A partir disso, foi determinado que o projeto operará com a resistência e facilidade de manutenção exigidas, conforme descrito nas normas AS 4100 e AS 3990, durante a vida útil do sistema acordada. Além disso, foi determinado que o sistema operará conforme necessário para todas as condições acordadas, ou seja, condições de operação normais, máximas, de inicialização e desligamento.

PALAVRAS-CHAVE: Estrutura deslizante. Transportador. Local de mina.

REFERÊNCIAS

Bharitkar, U.D., Kale, S.R., Agarwal, A.V., Lodha, B.R., Deshpande, S.P. (2015). **A Structured Approach to Material Handling System Selection and Specification for Manufacturing. International Journal of Advances in Mechanical and Civil Engineering**. 2, 91-95.

Dakhole, M. Y., Mehar, P. G., & Mujbaile, V. N. (2012). **Design and Analysis of Dedicated Fixture with Chain Conveyor Arrangement for Multistage Special Purpose Machine**. 2, 181-192.

Dunlop, F. (2009). Conveyor Handbook" conveyor belting,". Australia (June 2009), 1-32.

Fonseca, D. J., Uppal, G., & Greene, T. J. (2004). **A knowledge-based system for conveyor equipment selection**. Expert systems with applications, 26(4), 615-623.

Golka, K., Bolliger, G., & Vasili, C. (2007). **Belt conveyors**: principles for calculation and design. K. Golka, G. Bolliger, C. Vasili.

http://gearboxselection.com/gearbox-selection (2019)

Khan, N. H., Sarkar, D. K., Siddique, A., Rahman, M. M., & Chakraborty, S. (2017). **Fabrication of a Conveyor Belt with Object Sorting and Counting Facility**. International Journal of Advancements in Research & Technology, 6(5), 60-64.

Lan, C. H. (2003). **The design of a multi-conveyor system for profit maximisation**. The International Journal of Advanced Manufacturing Technology, 22(7-8), 510-521.

Lorbrand: Conveyor Pulleys. Available: https://www.lorbrand.com.au/work/pulleys (2019)

Lorbrand, Idler Catalogue, www.lorbrand.com

Marland Clutch: Backstop to Prevent Reversal of Inclined Conveyor and Vertical Bucket Elevators. Braintree, Massachusetts

ME4521: Bulk Materials Handling. Lecture 10, Belt Conveyors, 2019

Nuttall, A. J. G., Lodewijks, G., & Breteler, A. K. (2006). **Modelling rolling contact phenomena in a pouch belt conveyor system**. Wear, 260(9-10), 1081-1089.

Opasiak, T., Gąska, D., Peruń, G., & Łazarz, B. (2014). **Influence construction of the roller on the power of the drive system of the belt conveyor**. Zeszyty Naukowe. Transport/ Politechnika Śląska, (84), 93-98.

Patil, V. M., Vidya, N. A., Katkar, R. L., & Pande, P. S. (2015). **Type of Conveyor System**: A Review. International Journal for Scientific Research and Development, 2, 305-307.

SEW-EURO Drive, (E)DRN. (IR3) Gearmotors-6oHz Catalog, (2016)

Shinde, S. M., & Patil, R. B. (2012). Design and Analysis of a Roller Conveyor System for Weight Optimization and Material Saving. Jawaharlal Nehru College of Engineering, Aurangabad,(MS)

International Journal on Emerging Technologies, 3(25).

Sivakumar, S., Ranjithkumar, N., & Ragunathan, S. (2013). Design and development of down draft wood gasifier. **International Journal of Mechanical Engineering**, 2(2), 1-10.

STANDARD DIN 22101 **Continuous conveyors-Belt conveyors for loose bulk materials-Basis for calculation and dimensioning**, pp. 1-56. Deutsches Institut fur Normung E.V. (DIN), Berlin (2011-12)